Modeling of Silicon and Silica Nanowires for Optical Sensing

A thesis submitted in partial fulfillment of the requirements for the degree of Bachelor of Science in Electrical Electronic and communication Engineering

by

Israt Rahman	Student ID: 201416022
Zakia Tamanna Tisha	Student ID: 201416042
Pragati Gupta	Student ID: 201416044

Under the supervision of

Dr. Md. Shah Alam
Professor, Department of Electrical and Electronic Engineering, BUET

Department of Electrical Electronic and Communication Engineering
Military Institute of Science and Technology
Mirpur Cantonment, Dhaka-1216

December, 2017

CERTIFICATION

This thesis paper titled Modeling of Silicon and Silica Nanowires for Optical Sensing submitted by the group mentioned below has been accepted as satisfactory in partial fulfillment of the requirements for the degree B. Sc. in Electrical Electronic and Communication Engineering on December 2017.

Supervisor

Dr. Md. Shah Alam
Professor
Dept of EEE, BUET

Group Members

Israt Rahman
Student ID: 201416022
EECE-12, MIST

Zakia Tamanna Tisha
Student ID: 201416042
EECE-12, MIST

Pragati Gupta
Student ID: 201416044
EECE-12, MIST

DECLARATION

It is hereby declared that the work presented in this thesis paper titled "Modeling of Silicon and Silica Nanowires for Optical Sensing" is an outcome of study, analysis, simulation and research work carried out by the undersigned group of students of Electrical Electronic and Communication Engineering (EECE-12), Military Institute of Science and Technology (MIST), Mirpur Cantonment, Dhaka-1216, under the supervision of Dr. Md. Shah Alam, Professor, Department of Electrical Electronic Engineering (EEE), Bangladesh University of Engineering and Technology, Dhaka, Bangladesh.

It is also declared that neither of this thesis paper nor any part of this has been submitted anywhere else for the award of any degree diploma or other qualifications.

Supervisor

Dr. Md. Shah Alam
Professor
Dept of EEE, BUET

Group Members

Israt Rahman
Student ID: 201416022
EECE-12, MIST

Zakia Tamanna Tisha
Student ID: 201416042
EECE-12, MIST

Pragati Gupta
Student ID: 201416044
EECE-12, MIST

ACKNOWLEDGEMENT

First of all, thanks to Almighty Allah for his blessings for the successful completion of our thesis.

Secondly, we would like to express our sincerest gratitude and appreciation to our supervisor Dr. Md. Shah Alam, Professor, Department of Electrical and Electronic Engineering, Bangladesh University of Engineering and Technology, Dhaka, Bangladesh for the great mentorship and encouragement he has provided us throughout the year. Completing this work would have been impossible if it were not for his constant supervision and guidance. We have been extremely lucky to have a supervisor who was incredibly patient with us and responded to our queries so promptly. He aided us to develop a good understanding of the topic and encouraged us to delve further into its subject matter. We are forever indebted to him for his valuable advices and most importantly, for believing in us.

Additionally, we are grateful to all other Professors, Staff as well as students of both Bangladesh University of Engineering and Technology (BUET) and Department of Electrical Electronic and Communication Engineering (EECE) of Military Institute of Science Technology (MIST) for their co-operation during the course of our thesis work.

And last but not the least, we are thankful to our families and dear mates for their continuous support throughout the entire process.

ABSTRACT

The unique optical and mechanical properties of nanowires have led to their widespread use as sensing devices. In this thesis, at first a study of the characteristics of silicon nanowire and silica nanowire have been presented using the full-vectorial finite element method on COMSOL Multiphysics. Description of variations of the effective indices, effective area and confinement factors alongside core radius for the fundamental mode and higher order modes for silicon nanowire and silica nanowire are presented in this work. Field distribution and power profile of both the nanowires are also shown. The silicon and silica nanowires have also been analyzed for non-linearity and group velocity dispersion. A Mach-Zehnder-based optical sensor was studied to observe optical sensing in Silica nanowire in the full-vectorial finite element method. Characteristics like propagation constant of reference arm, propagation constant difference and power fraction have been described as function of core diameters. Finally, the sensitivity of the optical sensor was studied against variations of the molar concentration for two different radii of nanowire range.

TABLE OF CONTENTS

LIST OF TABLES

LIST OF FIGURES

CHAPTER 1

INTRODUCTION

1.1. Nanowire and Nanotechnology

Nanowire is an extremely thin wire with a diameter on order of a few nanometers (nm) or less [1]. It is a nanostructure that has the ratio of length to width greater than 1000. In preference, nanowire can be described as structure those have a thickness constrained to tens of nanometers or less and an unconstrained length. So the aspect ratio of a nanowire is of 1000 or more. It is a wire of dimensions of the order of a nanometer (10^{-9} meters) and it is also known as 'quantum wire' as at this scale quantum mechanical scales are important. Because of the aspect ratio of nanowires, sometimes nanowires are considered as 1-D (one dimensional) materials. Nanowires lead to some unique properties that are not seen in bulk or 3-D (three dimensional) material. This is because electrons in nanowires are quantum confined laterally and thus occupy energy levels that are different from the traditional continuum of energy levels or bands found in bulk materials [2]. Nanowires are considered as key nanomaterials because of their electrical controllability for accurate measurement, and chemical-friendly surface. Nanotechnology is the manipulation of matter on an atomic, molecular and supermolecular scale. Nanotechnology is considered to be in authority of matter at dimensions of approximately 1 to 100 nanometers.

Recently, one-dimensional (1D) nanostructures have attracted significant attention due to their advanced properties over those of the bulk material. Thus, shape control of the nanostructure is an important issue because the physical and chemical properties of the nanostructures are dependent on their dimensions and shape. In addition, structural modification of the nanowires is expected to provide a wider range of functionalities and improve device performance with respect to the assembly of the nanowires into more complex superstructures [3]. Nanowires often show noncrystalline order. Because of lack of crystalline order, a nanowire is periodic only in one direction. Hence it can

assume any order in the other directions (in plane) if this is energetically favorable. Large evanescent fields, high-nonlinearity, strong confinement, and low-loss interconnection to other optical fibers and fiberized components are some optical and mechanical properties of optical nanowires. Optical fiber nanowires (OFNs) with surface roughness and high-homogeneity provide low optical loss and allow the use of nanowire for a vast range of applications. Nanowires are identical to normal electrical wires other than the fact that they are extremely small [4]. Nanowires can be categorized by the materials as follows:

- Metal nanowire
- Semiconductor nanowire
- Oxide nanowire
- Multi-segment nanowire

1.2. Properties of Nanowire

Depending on the material used as nanowire, the properties of nanowire can have huge varieties. Nanowires are promising materials for many novel applications not only because of their geometry, but also because they possess many unique properties, such as:

- Electrical properties
- Optical properties
- Thermal properties
- Mechanical properties

Considering the electrical properties of nanowires, in 1-D system such as nanowire has remarkable properties and potential in nanoscale electronics devices. They are often configured in field effect transistor structure. Important factors that it reminds transport properties of nanowire which includes core diameter which is important for both classical and quantum size effects material composition, surface condition, crystal quality and the crystal orientation along the wire axis of the material. Electronic transport phenomena in one dimensional system can be roughly divided into two categories. First one is ballistic transport and the second one is diffusive transport. Ballistic transport phenomena occurs when the electrons can travel across the nanowire without a scattering. This only happens for short nanowires with length diameter to the

mean free path of the carrier or the electrons. For nanowires with length much larger than the carrier mean free path the electrons or on the other hand the holes and they are gone numerous scattering event when they travel along the wire. This case the transport is in the diffusive regime and the conduction is dominated by the carrier scattering with in the wire. 1-D nanostructure represents the smallest dimension structure that can efficiently transport electrical carriers.

For optical properties of nanowire, controlling the flow of optically encoded information with nm-scale accuracy over distance of many microns may find applications in future high density optical computing. Devices that are based on optically sensitive nanowires have a high potential for photovoltaic cells. Organic nanowire phototransistors exhibits interesting photoelectronic properties upon different light radiation. This nanowire yields higher photoconductive gains and external quantum efficiencies. Single crystal nanowires are a highly promising alternative to conventional thin film type photodiodes and can be effectively pave the way for optoelectronic device.

For the thermoelectric properties, heat produced by infrared photons emitted by the sun is currently not harvested and represents lost energy [4]. Additionally, heat from car braking and the engines is not being efficiently utilized. Bulk materials are considered as poor thermoelectric device because its thermal conductivity is too high. As a nanowire shrinks in size, the surface atoms becomes more numerous compared to the atoms within the nanowire, and edge effects become more important. Defects and scattering including edge effects are caused when nanowire width is below the free electrons mean free path of the wire material, means nanowires made from metals can have conductivity much lower than that for the bulk material. The mechanical properties of the nanowires are the most highly structure dependent. 1-D single crystalline nanostructure are very strong and exhibits very low number of defects per length.

1.3. Application of Nanowire

During the past decade, nanowires have attracted an enormous interest due to a large variety of promising applications in areas such as nanoelectronics, biotechnology, magnetism, thermoelectric, solar cells, and water splitting, among others. Their reduced

size, elongated geometry, and high surface-to-volume ratio turn nanowires into ideal elements for electrical and electrochemical systems. In addition, nanowires are considered excellent model objects to study how fundamental physical properties (such as mechanical, optical, electronic, thermoelectrical and magnetic) depend on dimension, composition, geometry and crystallinity of the nanostructures. In recent days nanowires are used in various research field.

1.3.1. Nanowire as sensor

Nanowire can be used as optical sensors as well as biosensor. The application of silicon nanowire (SiNW) as a sensing nanomaterial for detection of biological and chemical species has gained attention due to its unique properties [5]. With the fast growth and development of advanced nanotechnology, many sensing nanomaterials with unique properties, desired size, and chemical compositions have been fabricated to be incorporated within the transducer. One of them is the application of one-dimensional (1D) properties, desired size, and chemical compositions have been fabricated to be incorporated within the transducer. One of them is the application of one-dimensional (1D) nanostructures (nanotubes, nanowires, nanorods, nanobelts and heteronanowires) within the transducers in previous studies that can enhance the sensor performance, for example, TiO_2 nanowires [6], carbon nanotubes [7], CuS nanowires [8], NiO-Au nanobelts [9], CuS nanotubes [7], and graphene oxide-modified vanadium nanoribbons [10].

Silicon nanowire is one of the 1D nanostructures and has emerged as the promising sensing nanomaterial upon its unique mechanical, electronical, and optical properties [11-15]. The main reason why SiNWs have attracted attention in the development of ultrasensitive sensors is due to their high surface to volume ratios [16, 17] thus greatly enhancing the detection limit to fM concentrations and giving high sensitivity. In addition, the dimension of SiNW is in the range of ≈1–100 nm, hence making it very comparable and compatible to the dimensional scale of biological and chemical species [18, 19]. Having the smallest dimension, SiNWs exhibited good electron transfer in detection because the accumulation of charge in SiNWs directly occurs within the bulk of material resulting in fast response of detection. Fig. 1.1 shows the advantage of the nanostructures for sensing biomolecules. Fig. 1.1(a) shows that, for sensing a given kind of target particles, in the cross sectional view, a greater percentage of the region

in the structure with a high surface to volume ratio is affected. That means most regions can be considered as sensing areas. However, for the situation with low surface to volume ratios, only limited region near the surface can respond to the target particles. In Fig. 1.1(b), nanostructures with blue backgrounds are used as supports to immobilize receptors or labels, those with yellow backgrounds function.

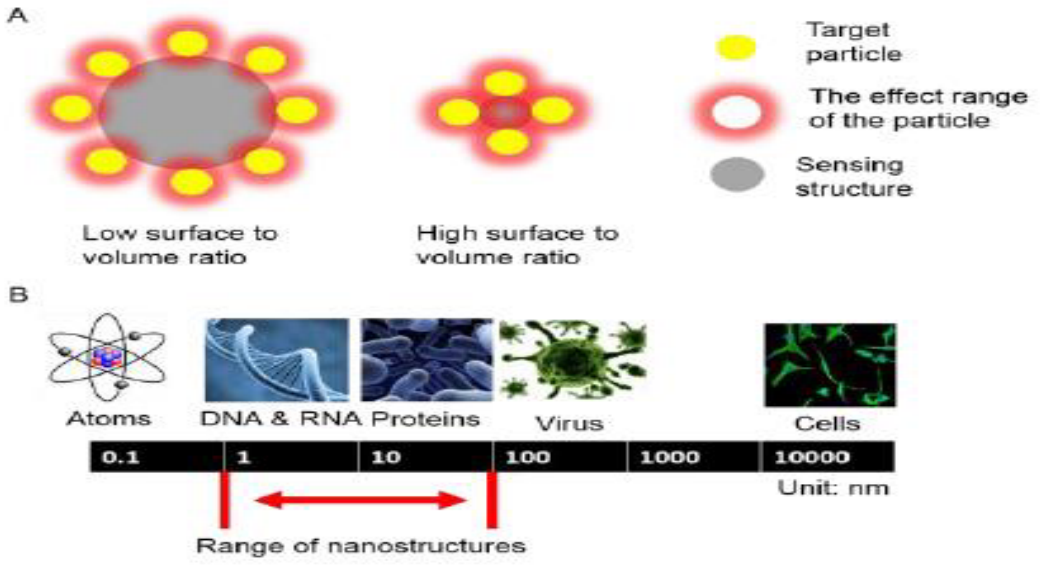

(a)

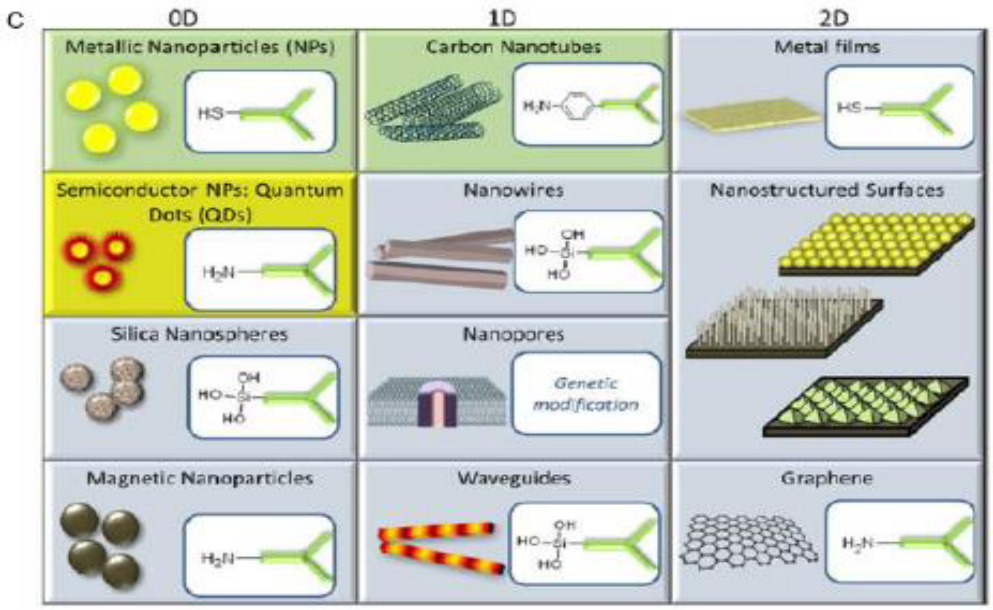

(b)

Fig. 1.1: (a) Schematic to illustrate the benefits of high surface to volume ratios and the size of nanostructures is comparable with several biomolecules. (b) An of nanostructures used in biological and medical applications.

as labels, and those with green backgrounds function as both labels and supports are shown. The insets in the white background show the major bioconjugation protocol used to immobilize receptors on the corresponding nanomaterial. The green antibody in the insets represents a generic biomolecule.

1.3.2. In electronics

- Developing a lead free solder reliable enough for space missions and other high stress environments using copper nanoparticles.
- Using electrodes made from nanowires that would enable flat panel displays to be flexible as well as thinner than current flat panel displays.
- Using semiconductor nanowires to build transistors and integrated circuits.
- Combining gold nanoparticles with organic molecules to create a transistor known as a NOMFET (Nanoparticle Organic Memory Field-Effect Transistor).
- Using carbon nanotubes to direct electrons to illuminate pixels, resulting in a lightweight, millimeter thick "nanoemmissive" display panel.
- Using self-aligning nanostructures to manufacture nanoscale integrated circuits.
- Using nanowires to build transistors without p-n junctions.
- Using buckyballs to build dense, low power memory devices.
- Using silver nanowires embedded in a polymer to make conductive layers that can flex, without damaging the conductor.
- IMEC and Nantero are developing a memory chip that uses carbon nanotubes. This memory is labeled NRAM for Nanotube-Based Nonvolatile Random Access Memory and is intended to be used in place of high density Flash memory chips.
- Using carbon nanotubes to direct electrons to illuminate pixels, resulting in a lightweight, millimeter thick "nanoemmissive" display panel.

1.3.3. In material

- By building an object atom by atom or molecule by molecule, molecular manufacturing, also called molecular nanotechnology, can produce new materials with improved performance over existing materials. For example, an airplane strut must be very strong and lightweight. A molecular fabricator could build the strut atom by atom out of carbon, making a lightweight material that is stronger than a diamond.

- A catalyst using platinum-cobalt nanoparticles is being developed for fuel cells that produces twelve times more catalytic activity than pure platinum.

1.3.4. In environment

- Generating less pollution during the manufacture of materials. One example of this is how researchers have demonstrated that the use of silver nanoclusters as catalysts can significantly reduce the polluting byproducts generated in the process used to manufacture propylene oxide.
- Producing solar cells that generate electricity at a competitive cost.
- Increasing the electricity generated by windmills. Epoxy containing carbon nanotubes is being used to make windmill blades. The resulting blades are stronger and lower weight and therefore the amount of electricity generated by each windmill is greater.
- Reducing the cost of fuel cells**.** Changing the spacing of platinum atoms used in a fuel cell increases the catalytic ability of the platinum. This allows the fuel cell to function with about 80% less platinum, significantly reducing the cost of the fuel cell.
- Clearing volatile organic compounds (VOCs) from air.
- Using photocatalytic copper tungsten oxide nanoparticles to break down oil into biodegradable compounds.

1.3.5. In medicine

- One application of nanotechnology in medicine currently being developed involves employing nanoparticles to deliver drugs, heat, light or other substances.
- Nanoparticles composed of polyethylene glycol-hydrophilic carbon clusters (PEG-HCC) have been shown to absorb free radicals at a much higher rate than the proteins out body uses for this function. This ability to absorb free radicals may reduce the harm that is caused by the release of free radicals after a brain injury.
- One of the earliest nanomedicine applications was the use of nanocrystalline silver which is as an antimicrobial agent for the treatment of wounds.
- Nanotechnology is used to identify cancer cells.

1.3.6. In energy

- Flexible layers of nanoporous germanium which can be used to produce lightweight solar cells for mobile applications.
- A type of Metal-Organic-Frameworks (MOFs) that has the ability to store natural gas which can be used to improve natural gas storage tanks for vehicles and allow wider use of natural gas to fuel cars.
- Producing high efficiency light bulbs. A nano-engineered polymer matrix is used in one style of high efficiency light bulbs.
- Generating steam from sunlight. It has demonstrated that sunlight, concentrated on nanoparticles, can produce steam with high energy efficiency. The "solar steam device" is intended to be used in areas of developing countries without electricity for applications such as purifying water or disinfecting dental instruments. Another research group is developing nanoparticles intended to uses sunlight to generate steam for use in running power plants [20].

Besides these applications, nanowires are being used as optoelectronic devices, memory devices advanced composite materials and etc.

1.4. Nanowire as Optical Waveguide

An optical waveguide is physical structure that guides electromagnetic waves in optical spectrum [21]. It is a propagation medium which confines, supports and guides energy of a propagating wave along a prescribed usually narrow and controllable path and usually consists of configuration of materials and usually affects the waves in some way during their propagation [22]. Generally waveguides include optical fiber. Nanowires are used in optoelectronics devices as waveguide. Because of the unique features of nanowire, it is becoming popular as optical waveguide. This structure is illustrated in Fig.1.2, which shows a transparent core with a refractive index n_1 surrounded by a transparent cladding of slightly lower refractive index n_2 and n_1 is greater than n_2. The cladding supports the waveguide structure while also, when sufficiently thick, substantially reducing the radiation loss into the surrounding air [23]. In essence, the light energy travels in both the core and the cladding allowing the associated fields to decay to a negligible value at the cladding–air interface. A guided optical wave propagates in the waveguide along its longitudinal direction.

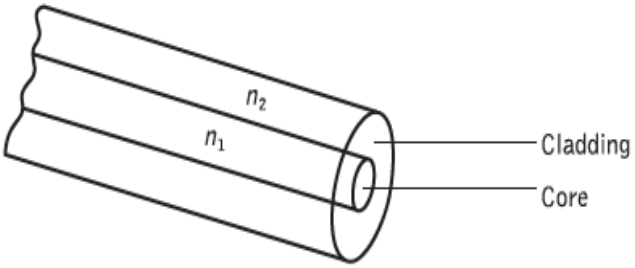

Fig. 1.2: Optical fiber waveguide showing the core of refractive index n_1, surrounded by the cladding of slightly lower refractive index n_2 [23].

1.5. Propagation of Light along a Nanowire

To consider the propagation of light within an optical fiber utilizing the ray theory model it is necessary to take account of the refractive index of the dielectric medium. The refractive index of a medium is defined as the ratio of the velocity of light in a vacuum to the velocity of light in the medium. A ray of light travels more slowly in an optically dense medium than in one that is less dense, and the refractive index gives a measure of this effect. When a ray is incident on the interface between two dielectrics of differing refractive indices (e.g. glass–air), refraction occurs, as illustrated in Fig 1.3(a). It may be observed that the ray approaching the interface is propagating in a dielectric of refractive index n_1 and is at an angle φ1 to the normal at the surface of the interface. If the dielectric on the other side of the interface has a refractive index n_2 which is less than n_1, then the refraction is such that the ray path in this lower index medium is at an angle φ_2 to the normal, where φ_2 is greater than φ_1 [23]. The angles of incidence φ_1 and refraction φ_2 are related to each other and to the refractive indices of the dielectrics by Snell's law of refraction which states that:

$$n_1 \sin \varphi_1 = n_2 \sin \varphi_2 \tag{1.1}$$

Or,
$$\frac{\sin\varphi_1}{\sin \varphi_2} = \frac{n_2}{n_1} \tag{1.2}$$

It may also be observed in Fig. 1.3(a) that a small amount of light is reflected back into the originating dielectric medium (partial internal reflection). As n_1 is greater than n_2, the angle of refraction is always greater than the angle of incidence. Thus when the angle of refraction is 90° and the refracted ray emerges parallel to the interface between the dielectrics, the angle of incidence must be less than 90°.

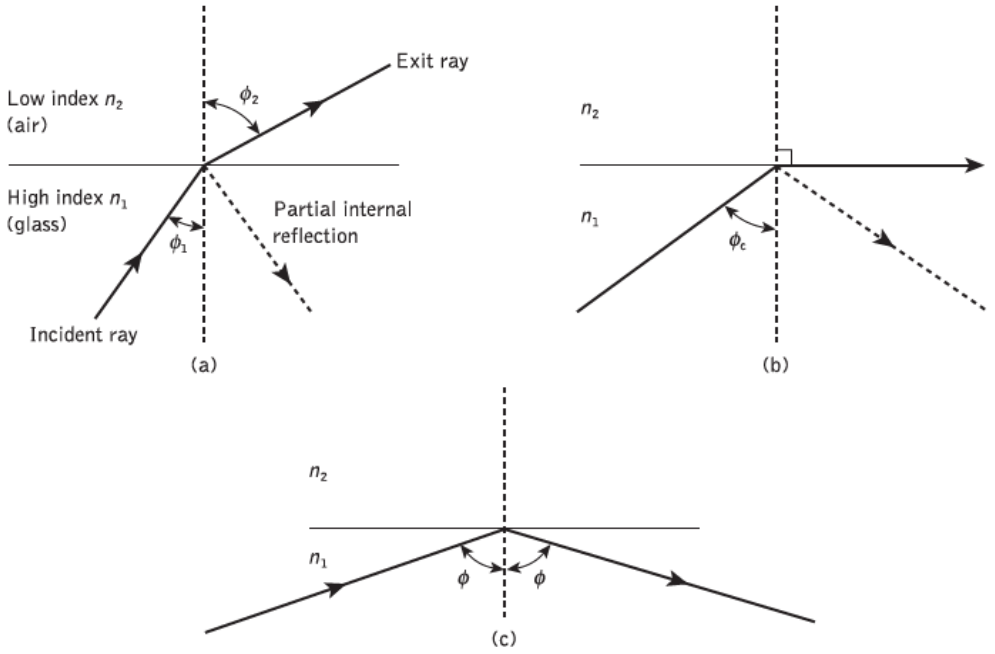

Fig. 1.3: Light rays incident on a high to low refractive index interface (e.g. Glass – air) (a) refraction; (b) the limiting case of refraction showing the critical ray at an angle φ_C; (c) total internal reflection where $\varphi > \varphi_C$.

This is the limiting case of refraction and the angle of incidence is now known as the critical angle φc, as shown in Fig. 1.3(b). From Eq. (1.2) the value of the critical angle is given by:

$$sin\ \varphi_C = \frac{n_2}{n_1} \tag{1.3}$$

At angles of incidence greater than the critical angle the light is reflected back into the originating dielectric medium (total internal reflection) with high efficiency (around 99.9%). Hence, it may be observed in Fig. 1.3(c) that total internal reflection occurs at the interface between two dielectrics of differing refractive indices when light is incident on the dielectric of lower index from the dielectric of higher index, and the angle of incidence of the ray exceeds the critical value. This is the mechanism by which light at a sufficiently shallow angle (less than $90° - \varphi_C$) may be considered to propagate down an optical fiber with low loss. Fig. 1.4 illustrates the transmission of a light ray in an optical fiber via a series of total internal reflections at the interface of the silica core and the slightly lower refractive index silica cladding. The ray has an angle of incidence, φ at the interface which is greater than the critical angle which is reflected at

the same angle to the normal.

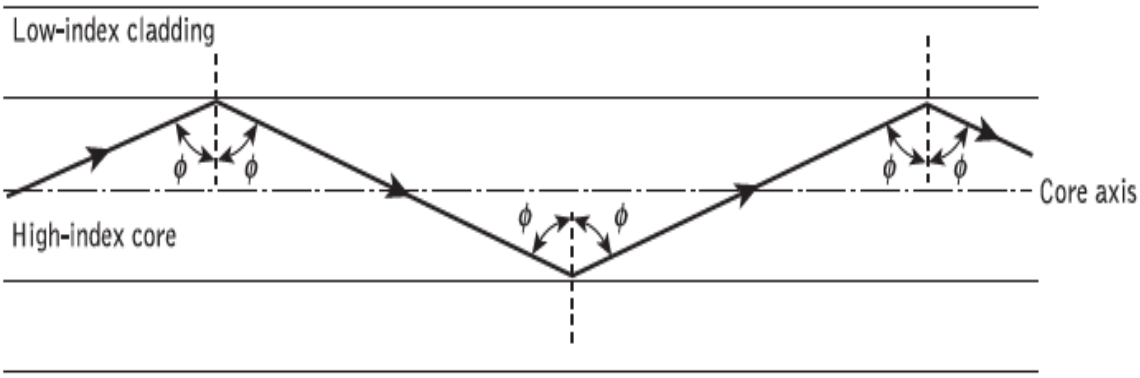

Fig. 1.4: The transmission of a light ray in a perfect optical fiber.

The geometry concerned with launching a light ray into an optical fiber is shown in Fig. 1.5, which illustrates a meridional ray *A* at the critical angle φ_C within the fiber at the core–cladding interface. It may be observed that this ray enters the fiber core at an angle θ_a to the fiber axis and is refracted at the air–core interface before transmission to the core–cladding interface at the critical angle. Hence, any rays which are incident into the fiber core at an angle greater than θ_a will be transmitted to the core–cladding interface at an angle less than φ_C, and will not be totally internally reflected.

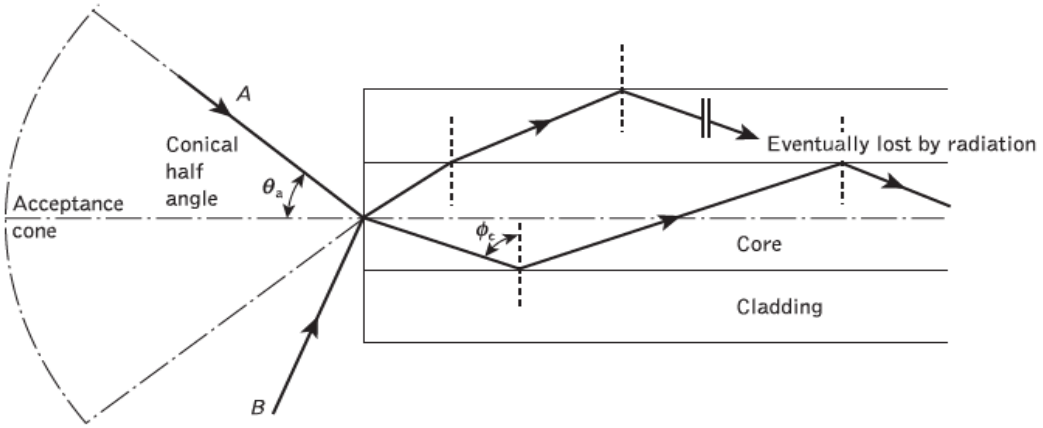

Fig. 1.5: The acceptance angle θa when launching light into an optical fiber.

This situation is also illustrated in Fig. 1.5, where the incident ray *B* at an angle greater than θ_a is refracted into the cladding and eventually lost by radiation. Thus for rays to be transmitted by total internal reflection within the fiber core they must be incident on the fiber core within an acceptance cone defined by the conical half angle θ_a. Hence θ_a is the maximum angle to the axis at which light may enter the fiber in order to be

propagated, and is often referred to as the acceptance angle for the fiber. If the fiber has a regular cross-section (i.e. the core–cladding interfaces are parallel and there are no discontinuities) an incident meridional ray at greater than the critical angle will continue to be reflected and will be transmitted through the fiber. From symmetry considerations it may be noted that the output angle to the axis will be equal to the input angle for the ray, assuming the ray emerges into a medium of the same refractive index from which it was input.

1.6. Nanowire as Optical Sensor

Earlier in section 1.3.1, it has been discussed that nanowire can be used as sensors. Evanescent-field-based optical waveguide sensors represents some important features in sensing applications. By means of measuring small changes in optical phase or intensity of the guided light, these sensors present excellent properties such as high sensitivity, fast response, immunity to electromagnetic fields, and safety in the detection of combustible and explosive materials. Along with increasing demands and rapid development of nanotechnology in various fields, the combination of nanotechnology, biology, chemistry and photonics opens new opportunities of developing optical sensors with subwavelength or nanometric structures. Recently, subwavelength-diameter silica nanowires have been demonstrated for guiding light within the visible and near infrared spectral ranges. Fabricated by taper-drawing of optical fibers, these wires show excellent diameter uniformity and atomic-level sidewall smoothness, making them possible to guide light with low optical losses. Light guided along such a nanowire leaves a large fraction of the guided field outside the wire as evanescent waves, making it highly sensitive to the index change of the surrounding medium.

1.7. Literature Review

Over the years, nanowire technology has garnered a wide range of interest among researchers as the nanowire concept has become a necessity and has led us to many new technologies. The large number of research works and research groups in this field is a testament to the aforesaid statement.

A large amount of the research works has focused on Silicon and Silica nanowire waveguides in view of facts like they are the most important photonic and optoelectronic materials within the near-infrared and visible ranges Both silica and the silicon nanowire waveguides can be easily fabricated with the accuracy of nanometer [24]. A lot have been studies on their optical and physical properties and they have typical values of moderate and high refractive indices. Silicon nanowire waveguides based on silicon-on-insulator (SOI) techniques have exhibited the high-density integration of optical circuits due to the strong light confinement from its high refractive-index contrast. As a result they have become the material of choice for designing opto-electronic integrated circuit devices. The power density of Silicon nanowire waveguide is higher than that of the conventional single-mode fiber by a factor of about 1000. Therefore, nonlinear optical effects easily occur when a low input power is used [25]. On the other hand, the nonlinear Kerr coefficient of silicon is still high, which strengthens the nonlinear ability of silicon nanowire waveguides. Many kinds of nonlinear effects, such as self-phase modulation, cross-phase modulation, stimulated Raman scattering, two-photon absorption (TPA), and four-wave mixing (FWM), have been observed in silicon nanowire waveguides [26]. Silicon particularly stands out as the material for building compact optical devices because of its low-cost and mature fabrication technology. Some of the devices based on Silicon include Raman lasers, amplifiers, all-optical switches, four wave mixers, logical gates, wavelength converters etc.

In waveguide applications the fabrication of quantum wire and the initiation of a number of studies in the Silicon photonics field has been made possible due to the small size and high index contrast of silicon core with silica cladding. It is expected that in the future, opto-electronic technology based on Silicon will thrive in ultrahigh-speed communication systems, sensing and optical computing.

To explore the features of nanowire waveguides, many remarkable research works have been conducted bearing in mind many different aspects. Basic guiding properties of subwavelength-diameter wires have been studied based on exact solutions of Maxwell's equations and numerical calculations by Limin Tong, Jingyi Lou, Eric Mazur. They have considered an air-clad silica wire and an air-clad silicon wire in this study [24]. The presence of strong longitudinal electric field (Ez) in Si nanowire

waveguides through numerical computation have been demonstrated by Jeffrey B. Driscoll, Xiaoping Liu, Saam Yasseri, Iwei Hsieh, Jerry I. Dadap, and Richard M. Osgood, Jr. [27]. Further a rigorous H-field based full-vectorial modal analysis has been carried out to characterize a high index contrast optical waveguide in the submicron scale more accurately by N. Kejalakshmy, Arti Agrawal, Yasin Aden, D. M. H. Leung, B. M. A. Rahman, K. T. V. Grattan [28]. For their study they have considered a cylindrical nanowire composed of a silicon core with silica cladding.

A very important course in nanowire study is the application of nanowire as sensors. A Mach-Zehnder based Optical sensor composed of a Silicon nanowire have been proposed in a study by J. Y. Lou, L. M. Tong, and Z. Z. Ye [29], where the sensitive component is absorbed in an aqueous solution have been inspected using a Bessel function field expansion. The study showed that optical nanowire waveguides are very promising for developing high-sensitivity optical sensors of significantly reduced sizes. An experiment by C. Themistos, M. Rajarajan, B. M. Azizur Rahman, and K. T. V. Grattan in 2009 analysed the optical properties of silica nanowires in a Mach-Zehnder-based optical sensor for detecting biomaterial specimens using the finite element method [30]. Further a Mach–Zehnder interferometer (MZI) coupled microring sensor with a high sensitivity and a large measurement range has been demonstrated by Jianwei Wang and Daoxin Dai [31]. A study conducted by Mohammad Mohebbi, Hadi Khormaei, and Rasul Rezaei analysed the Mach-Zehnder interferometer in the infrared region of the spectrum [32]. The interferometer was assembled with two single-mode subwavelength diameter silica wires immersed in acetonitrile. At present a lot of research works are going on to set new benchmarks in the field of nanowire waveguides and optical sensing.

1.8. Objective of the Thesis

- To study the different properties of silicon Nanowire as nanowire waveguide and analysis of silicon nanowire.
- To study the different characteristics of silica Nanowire
- To find out the different features and characteristics of Silica Nanowire as optical sensor.

1.9. Thesis Outline

This thesis work is arranged in five chapters. All the chapters share the same reference list at the end of the thesis.

Chapter one consists of the introduction of nanowire and the applications of nanowire in various technical field. Later on this chapter we have discussed the use of nanowire as optical sensor. Along with nanowire features of general waveguide are also mentioned in this chapter. A brief description of the previous work has also been stated.

In chapter two, we have discussed about the analysis technique of silicon nanowire. A rigorous full-vectorial finite element method has been used to characterize such the nanowires. Starting from the brief history of finite element method, we described its solution process, principle, necessity and application. Then we represented COMSOL Multiphysics which is the simulation software which has been used to analyze. The advantage and preference for COMSOL Multiphysics is also discussed here. In the end of the chapter the designing process of nanowire is described.

In chapter three, the description of characteristics of nanowire are discussed. Effective index, effective are, confinement factor, hybridness, dispersion, nonlinearity are discussed among various characteristics of Silica nanowire. Corresponding equations and their evaluation is also given. The purpose of this discussion is to give a basic understanding of the properties we analyzed.

In chapter four, we have shown the results and discussions of different properties of silicon nanowire and silica nanowire respectively. Different modes of the nanowires have been studied. Different properties are explained with the help of graphs and necessary figures. The equations used for analysis have already been described in chapter three. Later on this chapter we showed the characteristics of Silica nanowire as optical sensor. We also presented the sensitivity and sensitive area of the nanowire.

Chapter Five has the conclusion part of the thesis work. We have also mentioned about some of the opportunities for future works those could help us discover more fascinating optical properties of nanowire.

CHAPTER 2

ANALYSIS TECHNIQUE

2.1. Finite Element Method

2.1.1. Introduction

The finite element method (FEM) is a numerical technique for solving physical problems which are described by partial differential equations or can be formulated as functional minimization. It is necessary to use mathematics to comprehensively understand and quantify any physical phenomena, such as structural or fluid behavior, thermal transport, wave propagation and the growth of biological cells. Most of these processes are described using Partial Differential Equations (PDEs). However, for a computer to solve these PDEs, numerical techniques have been developed over the last few decades and one of the most prominent today is the Finite Element Method. FEM was originally developed to study stresses in complex aircraft structures; it has since been extended and applied to the broad field of continuum mechanics, including fluid mechanics and heat transfer. Because of its capability to handle complex problems and its flexibility as an analysis tool, FEM has gained a prominent role in engineering analysis and design.

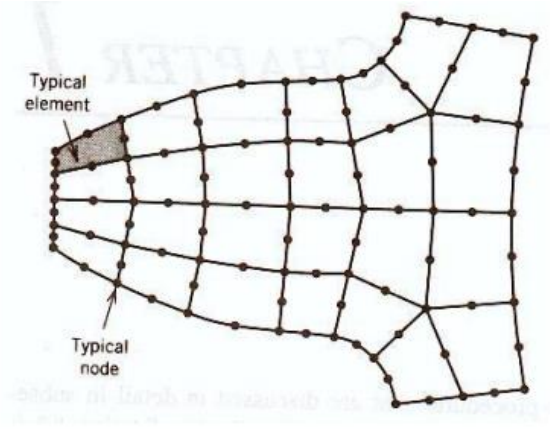

Fig. 2.1: Discretization of a structure

FEM mainly cuts a structure into several elements (pieces of the structure) which is known as 'discretization' and then reconnects elements at "nodes" as if nodes were pins that hold elements together Fig 2.1. This process results in a set of simultaneous algebraic equations [33]. Increasing the number of elements we can achieve any precision.

2.1.2. Principle of FEA

The finite element method (FEM) is a computational technique used to obtain approximate solutions of boundary value problems in engineering. Boundary value problems are also called field problems. The field is the domain of interest which is most often a physical structure represented as an assembly of 'finite elements'. The field variables are the dependent variables of interest governed by the differential equation. The boundary conditions are the specified values of the field variables or related variables such as derivatives on the boundaries of the field. For simplicity we assume a two-dimensional case with a single field variable φ(x, y) to be determined at every point P(x, y) such that a known governing equation is satisfied exactly at every such point. A node is a specific point in the finite element at which the value of the field variable is to be explicitly calculated [34].

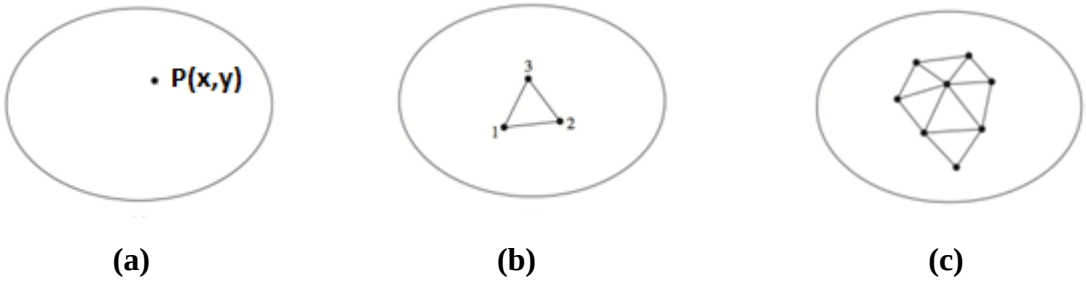

Fig. 2.2: (a) A general 2-D domain of field variable φ(x, y). (b) A 3 node finite element defined in that domain. (c) Additional elements showing a partial element mesh of the domain.

The values of the field variable computed at the nodes are used to approximate the values at non-nodal points that is in the element interior by interpolation of the nodal values. For the three-node triangle example, the field variable is described by the approximate relation,

$$\varphi(x,y) = N_1(x,y).\varphi_1 + N_2(x,y).\varphi_2 + N_3(x,y).\varphi_3 \quad (2.1)$$

Where, φ_1, φ_2 and φ_3 are the values of the field variable at the nodes, and N_1, N_2 and N_3 are the interpolation functions, also known as shape functions or blending functions. In the finite element approach, the nodal values of the field variable are treated as unknown constants that are to be determined. The interpolation functions are most often polynomial forms of the independent variables, derived to satisfy certain required conditions at the nodes. The interpolation functions are predetermined known functions of the independent variables and these functions describe the variation of the field variable within the finite element.

2.1.3. Steps of Finite Element Procedure

1. **Discretize the continuum:** The first step is to divide a solution region into finite elements. The finite element mesh is typically generated by a preprocessor program. The description of mesh consists of several arrays main of which are nodal coordinates and element connectivities.

(a) **(b)**

Fig.2.3: (a) Making nodes (b) Building elements by assigning connectivity.

2. **Select interpolation functions:** Interpolation functions are used to interpolate the field variables over the element. Often, polynomials are selected as interpolation functions. The degree of the polynomial depends on the number of nodes assigned to the element.
3. **Find the element properties:** The matrix equation for the finite element should be established which relates the nodal values of the unknown function to other parameters. For this task different approaches can be used; the most convenient are: the variational approach and the Galerkin method [35].
4. **Assemble the element equations:** To find the global equation system for the whole solution region we must assemble all the element equations. In other words we must combine local element equations for all elements used for discretization. Element connectivities are used for the assembly process. Before solution, boundary conditions and loads should be imposed.
5. **Solve the global equation system:** The finite element global equation system is typically sparse, symmetric and positive definite. Direct and iterative methods

can be used for solution. The nodal values of the sought function are produced as a result of the solution.

6. **Compute additional results:** In many cases we need to calculate additional parameters. For example, in mechanical problems strains and stresses are of interest in addition to displacements, which are obtained after solution of the global equation system.
7. **Accuracy**: In FEA only model of the real problem is solved. A good finite element model, once set up, is about a 95% accurate solution of the field equations, which themselves are based on a theoretical model, which is idealized from reality. So it is better to refine the mesh in areas of high stress, repeat the procedure for multiple times and check the iteration effects Fig. 2.4.

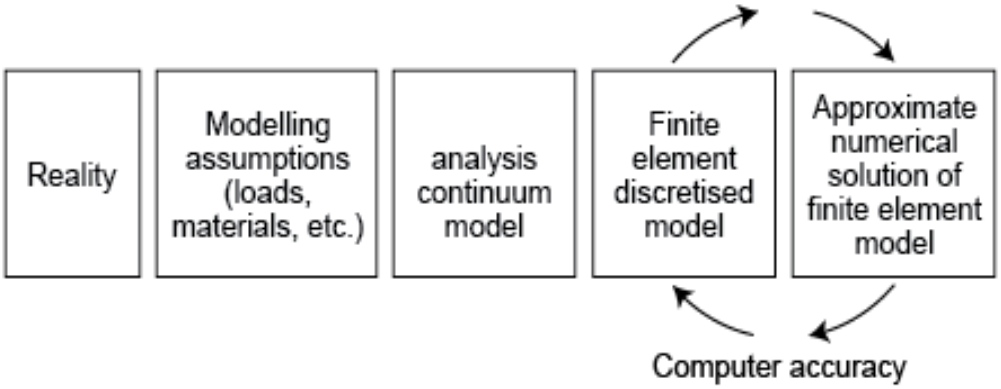

Fig 2.4: Finite Element Model process and accuracy [36].

2.1.4. Applications

FEM can handle problems possessing any or all of the following characteristics:

- Any mathematical or physical problem described by the equations of calculus, e.g. differential, integral, integro-differential or variational equations.
- Boundary value problems also called equilibrium or steady-state problems, Eigen problems for resonance and stability phenomena and initial value problems like diffusion, vibration and wave propagation.
- The domain of the problem may be any geometric shape, in any number of dimensions such as 1-D, 2-D or 3-D.
- Physical properties e.g. density, stiffness, permeability, conductivity may also vary throughout the system.
- The external influences, generally referred to as loads or loading conditions, may be in any physically meaningful form, e.g. pressure, thermal, inertial forces etc. The loads are typically applied to the boundary of the system (boundary

conditions), to the interior of the system (interior loads) or at the beginning of time (initial conditions).

- Problems may be linear or non-linear.

2.1.5. Advantages of FEM

- Can handle a wide variety of engineering problems. For Example: solid mechanics, dynamics, heat problems, fluids, electrostatic problems.
- Complex restraints and indeterminate structures can be solved.
- Optimizing product performance and cost
- Reduction of development time
- Elimination or reduction of testing
- First-time achievement of required quality
- Improved safety
- Satisfaction of design codes
- Improved information for engineering decision making
- Understanding of components allowing more rational design
- Satisfaction of legal and contractual requirements.

2.2. COMSOL Multiphysics

Finite element methods are extensively used in science and engineering applications based on approximations of partial differential equations. Numerical analysis tools make the solutions of coupled physics, mechanics, chemistry, and even biology accessible to the novice modeler. COMSOL is a very notable software for finite element analysis. It was started in July 1986 by Svante Littmarck and Farhad Saeidi at the Royal Institute of Technology (KTH) in Stockholm, Sweden. COMSOL Multiphysics (an acronym for Common Solution) is a cross-platform finite element analysis, solver and multiphysics simulation software [37]. Preprocessing and post processing was the main concern while designing the COMSOL Multiphysics software. FEA Software package for a variety of physics and engineering applications, specially coupled phenomena, or multiphysics. COMSOL Multiphysics also offers a widespread interface to MATLAB and its toolboxes for a large variety of programming, preprocessing and postprocessing

possibilities. The packages are cross-platform. COMSOL Multiphysics also permits for entering coupled systems of partial differential equations (PDEs) [38].

The uniqueness of COMSOL Multiphysics, over other FEA (Finite Element Analysis) software packages is its ability to solve coupled phenomena. These are phenomena for which the solution of each individual physical problem cannot be obtained independently of the others. Examples of these include combined fluid dynamics/chemical engineering or heat transfer/mechanical engineering problems [39].

2.2.1. Features of COMSOL Multiphysics

COMSOL Multiphysics offers unique user-friendly working environment and also provides wide range of tools for the fast and the effective analysis. There are numerous important features of the software. These are given below:

1. graphical user interface,
2. tools for creating the geometry and internal boundaries and domains,
3. automatic mesh generation and refinement,
4. the ability to solve different equations on different meshes,
5. the multi-physics capability which permits addition of equations to represent additional phenomena,
6. the ability easily to make parameters depend upon the solution,
7. the parametric solver and
8. the post-processing graphical features [40].

2.2.2. Modeling environment

COMSOL Multiphysics is a powerful interactive environment for modeling and solving all types of scientific and engineering problems which are based on partial differential equations (PDEs). With this software one can easily extend conventional models for one type of physics into multiphysics models that solve coupled physics phenomena and do so simultaneously. Accessing this power does not need any depth knowledge of mathematics or numerical analysis [41]. To built-in physics modes it is possible to build models by defining the relevant physical quantities such as material properties, loads, sources, fluxes and constraints rather than by defining the equations. COMSOL Multiphysics then internally compiles PDEs set that representing the entire model. Comsol Multiphysics has unique features in representing multiply linked domains with complex geometry, highly coupled and nonlinear equation systems, and arbitrarily

complicated boundary, auxiliary, and initial conditions. But with this modeling power comes great opportunities and great perils [42].

2.2.3. COMSOL Multiphysics and its importance

For long scientists and engineers have had to make assumptions in order to be capable of realize their design ideas. With the progression of time these assumptions are being refined and in some cases even eliminated to get more accurate results. Multiphysics is one major enabler to eliminate assumptions, by coupling related physical applications together to include all the necessary factors for a complete model. COMSOL Multiphysics is a simulation software designed to provide the most accurate results by minimizing the assumptions its users must make [43]. COMSOL Multiphysics users are free from the restrictive nature which generally associated with simulation software. The COMSOL user has full control of their model. The ability to couple any number of physics together and input user-defined physics and expressions directly into a model allows COMSOL users to be creative in a way which is not possible with other simulation software. So features of COMSOL have a great deal of flexibility when dealing with any physical problem. It is the greatest of them all, the ability to define user's own physics, in the form of PDEs for any kinds of problem. The ability to give any arbitrary PDE does not guarantee that its solvers would be able to solve it. Some of the advantages of the software have been briefly stated below:

- easy, seamless interface between heat transfer and other physics fields,
- ability to modify governing equations and
- flexibility in selection in the form of direct, iterative, or mixed solvers, and segregated, or fully coupled solutions [44].

2.2.4. Mesh refinement

COMSOL primarily uses the finite element method (FEM) to compute single and multiphysics simulations. Whenever using the finite element method, it is important to remember that the accuracy of the solution is linked to the mesh size. As mesh size decreases towards zero (leading to a model of infinite size), one has to move toward the exact solution for the equations they are solving. However, since one is limited by finite computational resources and time, they will have to rely on an approximation of the real solution. The objective of simulation is to minimize the difference ("error")

between the exact and the approximated solution, and to ensure that the error is below some accepted tolerance level that will vary from project to project based on your design and analysis goals.

We need to track a characteristic output parameter from our simulation as we vary the mesh size and determine at which mesh size the parameter has converged on the correct value. However convergence criteria will depend on design and analysis goals. Finer element size is chosen for mesh analysis [45].

2.2.5. Study of a nanowire in COMSOL version 4.4

We have designed a silicon nanowire using COMSOL 4.4 to analyze its different characteristics. These characteristics include effective mode index, effective area, electric field components, magnetic field components, confinement factor, pointing vector, power flow, polarization etc. COMSOL with MATLAB was also used for observing different outputs of silicon nanowire. The FEM in COMSOL study engaged the RF module; the function of the RF module is to combine the optics and photonics interfaces. In the RF module, to design a silicon nanowire we selected electromagnetic waves, frequency domain which shown in Fig. 2.5.

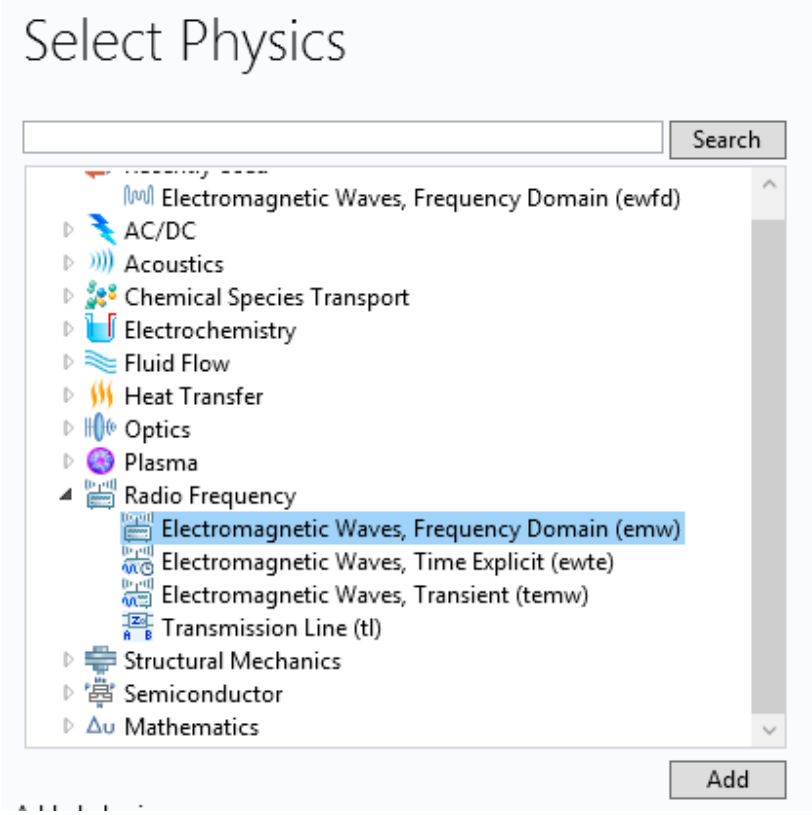

Fig.2.5: Selecting RF module using COMSOL version 4.4.

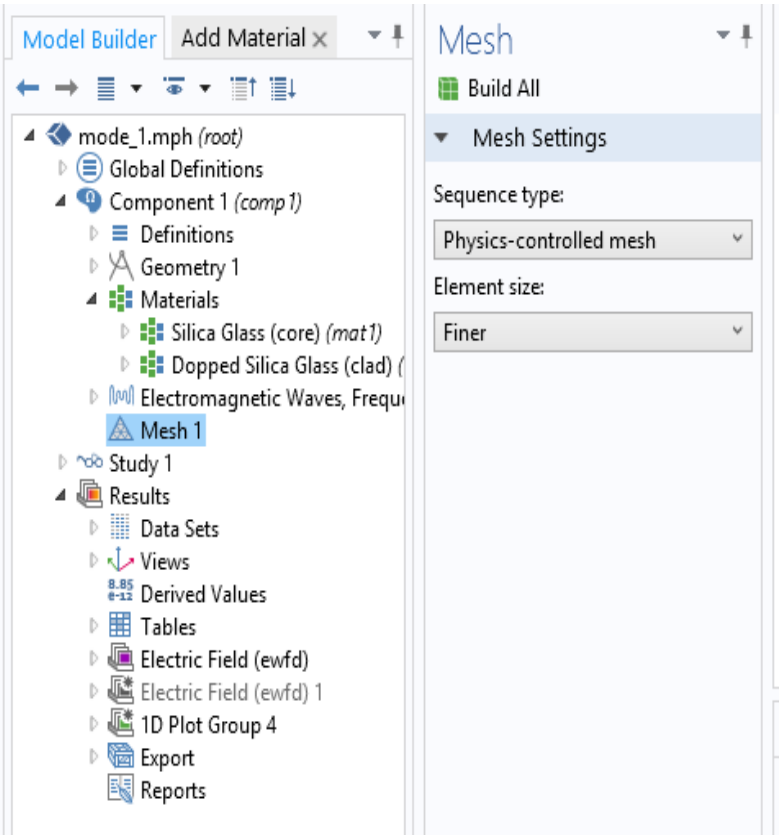

Fig. 2.6: Selecting sequence-type and element size for mesh analysis.

Some material properties were used as default in the study which are presented in Table 2.1. These properties are valid for the free space wavelength of 1.55 μm, which is in the infrared region where most of the fiber optic communication takes place. Modal analysis of the nanowire was performed as a part of the study. Associated sweeps were done to examine the dependency of the nanowire performance on the core radius. The core radius was varied from 0.2 to 1.4 μm. In this setting, the corresponding electric field intensities and effective refractive indices were determined for various values of core radius. The standard meshing tool was used with the mesh sequence type selected as physics-controlled mesh and element size was tuned to "finer". Fig. 2.6 shows selection of standard mesh analysis from model builder window and Fig. 2.7 shows the meshed geometry of the silicon nanowire cross section in 2D.

Table 2.1. Material properties used in the study

	Core	Cladding
Material	Silicon	Doped Silica Glass
Refractive Index	3.4754	1.444

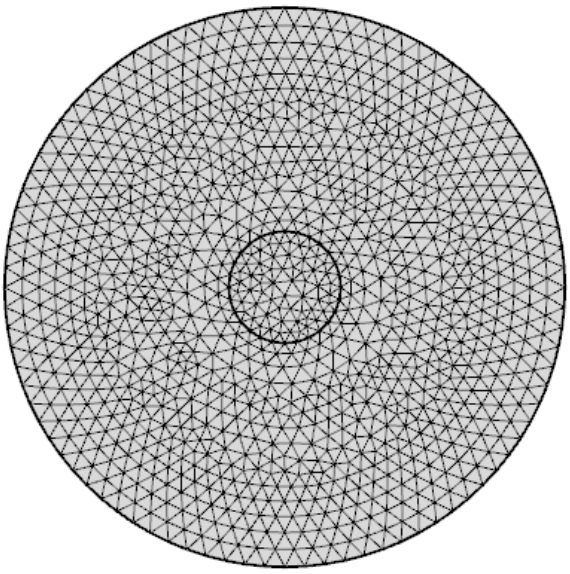

Fig. 2.7: Structure of the FEM in COMSOL for a silicon nanowire.

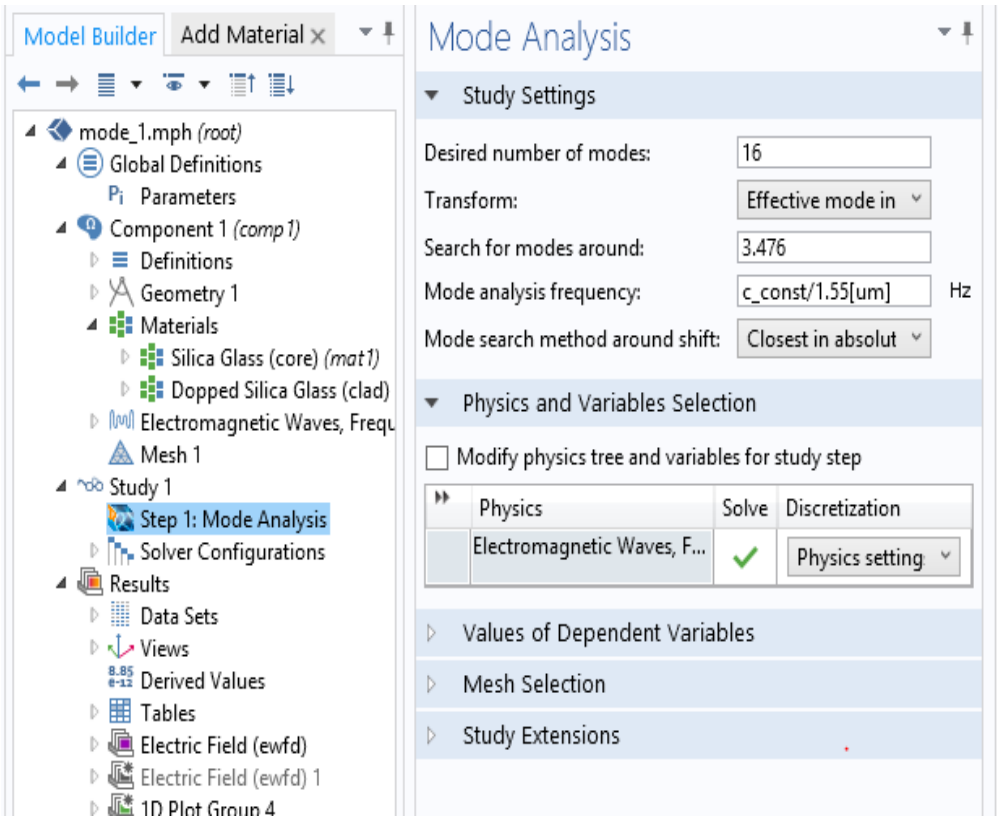

Fig. 2.8: Selection of effective mode index and mode analysis frequency.

Effective mode index lies between the refractive indices of the two materials. Fundamental mode has the maximum index. Hence to find the fundamental mode certainly, the mode index is set to search around the core index. Mode analysis

frequency can be obtained corresponding to a free space wavelength of 1.55 μm which has been shown in Fig. 2.8. Then after computing the analysis and changing the expression from the setting window for solution we obtained the result.

.

CHAPTER 3

MODAL ANANLYSIS OF SILICON AND SILICA NANOWIRE

To reveal some of the interesting features of nanowire waveguides, some important characteristics of Silicon and Silica have been studied. This chapter gives a brief discussion of these characteristics. The structure to be analyzed here is assumed to be uniformly extended up to infinity along z-direction and the refractive index and magnetic permeability are invariant along this direction. In order to obtain an improved model for the propagation of light in a waveguide, electromagnetic wave theory must be considered. The basis for the study of electromagnetic wave propagation is provided by Maxwell's equations. All the field components are assumed to have functional form of exp(i(ωt-βz)) and the governing wave equations, which is deduce form the Maxwell's equations in terms of the electric field vector $\vec{E}$ takes the form,

$$\overrightarrow{\nabla} \times \frac{1}{\mu_r} \overrightarrow{\nabla} \times \vec{E} - {K_0}^2 \varepsilon_r \vec{E} = 0 \qquad (3.1)$$

where is the dielectric constant of the medium which is complex for metal and lossy materials, is the relative permeability of the medium, is the free space wave number, is the angular frequency and β is the propagation constant.

3.1. Modes in a Planar Guide

The planar guide is the simplest form of optical waveguide. To visualize the dominant modes propagating in the *z* direction we may consider plane waves corresponding to rays at different specific angles in the planar guide. These plane waves give constructive interference to form standing wave patterns across the guide following a sine or cosine formula. Figure 3.1 shows examples of such rays for m =1, 2, 3, together with the electric field distributions in the *x* direction. It may be observed that *m* transverse electric (TE) field patterns of three lower order models (m = 1, 2, 3) n the planar dielectric guide denotes the number of zeros in this transverse field pattern. In this way *m* signifies the order of the mode and is known as the mode number. When light is

described as an electromagnetic wave it consists of a periodically varying electric field E and magnetic field H which are orientated at right angles to each other.

The transverse modes shown in Figure 3.1 illustrate the case when the electric field is perpendicular to the direction of propagation and hence E_Z= 0, but a corresponding component of the magnetic field H is in the direction of propagation. In this instance the modes are said to be transverse electric (TE). Alternatively, when a component of the E field is in the direction of propagation, but H_Z = 0, the modes formed are called transverse magnetic (TM). The mode numbers are incorporated into this nomenclature by referring to the TE_m and TM_m modes, as illustrated for the transverse electric modes shown in Figure 3.1. When the total field lies in the transverse plane, transverse electromagnetic (TEM) waves exist where both E_Z and H_Z are zero. However, although TEM waves occur in metallic conductors (e.g. coaxial cables) they are seldom found in optical waveguides.

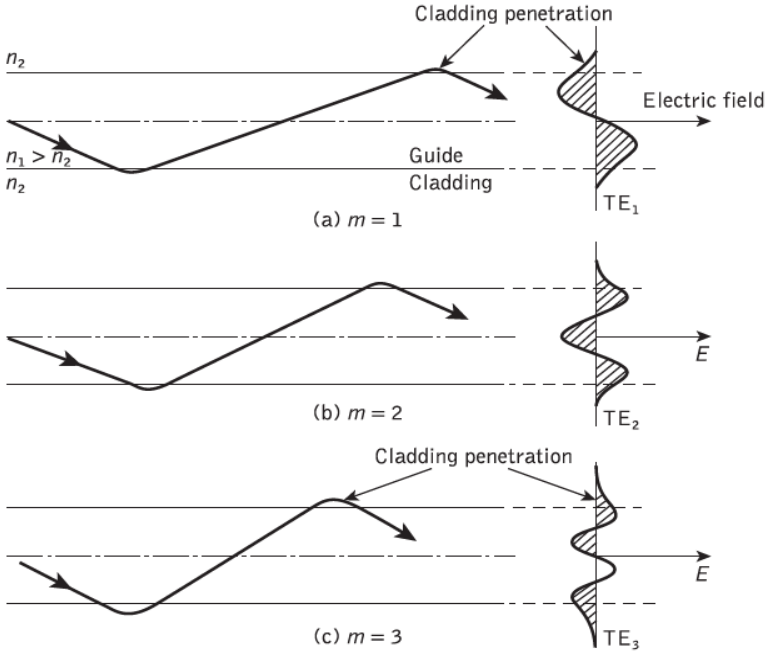

Fig. 3.1: Physical model showing the ray propagation and the corresponding transverse electric (TE) field patterns of three lower order models (m=1, 2, 3) in the planar dielectric guide. Denotes the number of zeros in this transverse field pattern.

Table 3.1 shows the relationship between the traditional HE, EH, TE and TM mode designations and the LP_m mode designations. The mode subscripts m and n are related to the electric field intensity profile for a particular LP mode. There are in general 2m

field maxima around the circumference of the fiber core and n field maxima along a radius vector. Furthermore, it may be observed from Table 3.1 that the notation for

Table 3.1. Correspondence between the lower orders in linearly polarized modes and the traditional exact modes from which they are formed

Linearly polarized	Exact
LP_{01}	HE_{11}
LP_{11}	HE_{21}, TE_{01}, TM_{01}
LP_{21}	HE_{31}, EH_{11}
LP_{02}	HE_{12}
LP_{31}	HE_{41}, EH_{21}
LP_{12}	HE_{22}, TE_{02}, TM_{02}
LP_{mn}	HE_{2n}, TE_{0n}, TM_{0n}
LP_{mn} ($m \neq 0$ or 1)	$HE_{m+1.n}$, $EH_{m-1.n}$

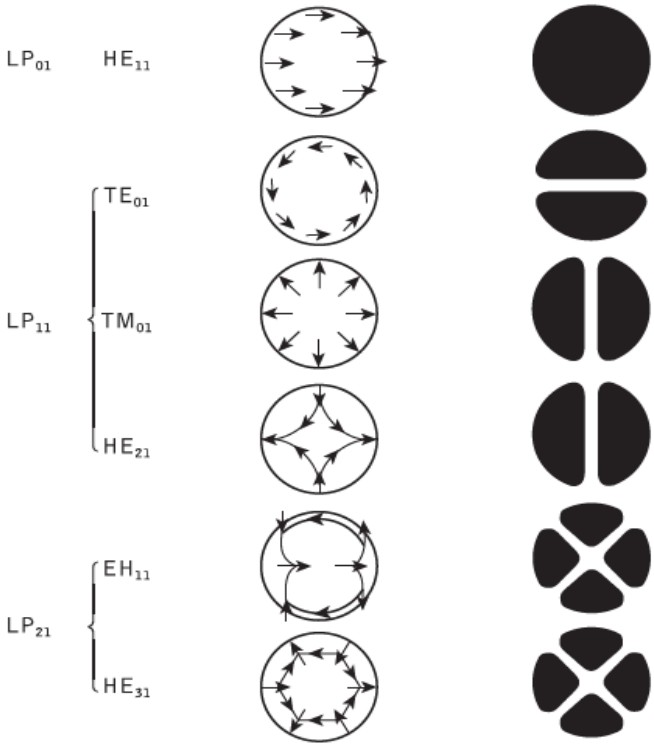

Fig. 3.2: The electric field configurations for the three lowest LP modes illustrated in terms of their constituent exact modes: (a) LP mode designations; (b) exact mode designations; (c) electric field distribution of the exact modes; (d) intensity distribution of E_x for the exact modes.

labeling the HE and EH modes has changed from that specified for the exact solution in the cylindrical waveguide mentioned previously. The subscript *m* in the LP notation now corresponds to HE and EH modes with labels m + 1 and m − 1 respectively. The electric field intensity profiles for the lowest three LP modes, together with the electric field distribution of their constituent exact modes, are shown in fig.3.2. It may be observed from the field configurations of the exact modes that the field strength in the transverse direction (E_x or E_y) is identical for the modes which belong to the same LP mode. Hence the origin of the term 'linearly polarized' [23].

3.2. Optical Fiber Types

A very important aspect in operating a fiber optic system is what type of optical fiber is being used and why. Understanding of the characteristics of the fiber types helps us to understand the applications for which they are used. Basically there are two types of fiber: multimode fiber and single-mode fiber. Multimode fiber is best suited for short transmission distances, so it is fit for use in LAN systems and video surveillance. Single-mode fiber is best designed for longer transmission distances, which makes it suitable for long-distance telephony and multichannel television broadcast systems [46].

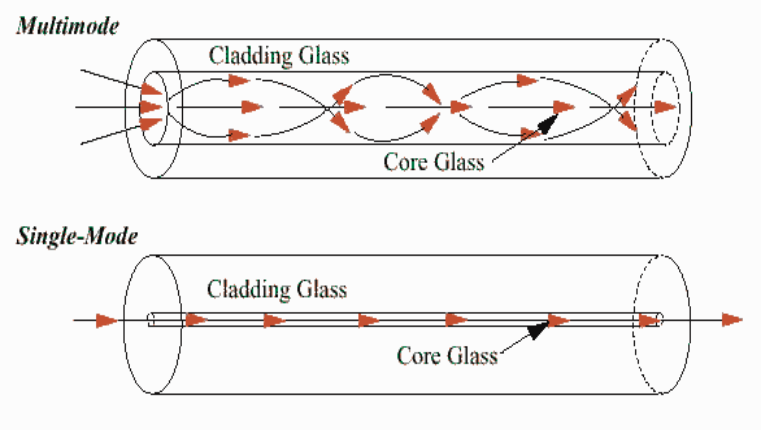

Fig. 3.3. Basic types of optical fiber.

3.2.1. Single mode fiber

Single mode fiber optic cable has a small diametric core that allows only a one mode of light to propagate. Because of this, the number of light reflections created due to the passing of the light through the core decreases, lowering attenuation and allowing the signal to travel further [47]. The cladding diameter is best designed to be 10 times the

core diameter to avoid losses from the evanescent field. With a coating and buffer jacket to provide protection and strength, single-mode fibers have almost similar overall diameters to multimode fibers.

This application is typically for transmission in long distance, making it ideally suited for high-bandwidth and medium- and long-haul applications using single-mode injection laser sources.

3.2.2. Multimode fiber

Multimode optical fiber has a large core that allows multiple modes of light to propagate. For this reason, the number of light reflections created due to the passing of the light through the core increases, allowing more data to pass through at a particular time.

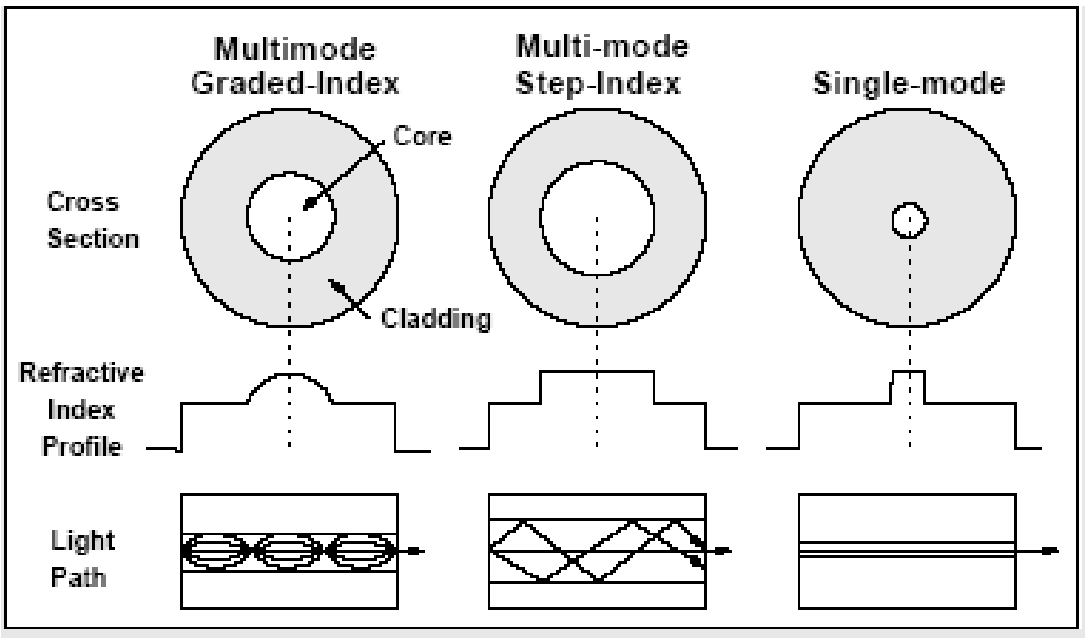

Fig. 3.4: Multi-mode Vs Single-mode Fiber [48].

3.2.3. Multimode step index fiber

As this fiber has a large core, some of the light rays that form the digital pulse may travel across a direct path, whereas others travel in zigzag as they bounce off the cladding. These alternate paths result in the different groups of light rays (which we refer as modes) that arrive separately at the receiving point. The pulse then begins to spread out, losing its distinct shape. The pulses are provided with spacing in between to prevent overlapping limits the amount of information that can be sent. These fibers can have reasonably large core diameters and large numerical apertures which enables

efficient coupling for incoherent light sources like LEDs. The performance characteristics of this fiber type may differ considerably depending on the materials used and the method of preparation; generally the doped silica fibers display the best performance. This type of fiber is best suited for transmission over short distances.

3.2.4. Graded-index multimode fiber

The core of a graded index multimode fiber has a distinct characteristic: the refractive index reduces gradually from the center axis out toward the cladding. The light rays moving down the axis travel more slowly than those near the cladding because of the higher refractive index at the center. Due to the graded index, light in the core curves helically rather than zigzag off the cladding, reducing its travel distance. The light at the periphery having higher speed and being allowed a shortened path arrive at a receiver at about the same time as those rays in the core axis. As a result, digital pulse suffers less dispersion. This type of fiber is best suitable for applications in local area networks (LAN). The performance characteristics of multimode graded index fibers are generally better than those for multimode step index fibers due to the index grading and lower attenuation. Multimode graded index fibers tend to have smaller core diameters than multimode step index fibers, although the inclusion of buffer jacket makes the overall diameter about the same. This gives the fiber greater firmness against bending.

3.3. Effective Index

Effective index is a characteristic property of the material. An effective refractive index for an optical waveguide provides us a measure of the overall phase delay of a light beam in it. We can define the refractive index *n* as the quantification of the phase change per unit length in a waveguide to that in vacuum [49]. Here, the phase delay per length is assumed to have been caused by the medium. The effective index n_{eff} has the analogous meaning for light propagation in a waveguide; the value of phase constant of the waveguide or β (for some wavelength) is the n_{eff} times the vacuum wavenumber. This relation can be expressed with the following equations:

$$\beta = n_{eff}\frac{2\pi}{\lambda} \tag{3.2}$$

Or, $$\beta = n_{eff}k_o \tag{3.3}$$

Or, $$n_{eff} = \frac{\beta}{k_0} \quad (3.4)$$

Here, $k_o (= \frac{2\pi}{\lambda})$ is the wavenumber and λ is the wavelength.

Usually in a single-mode fiber, the effective refractive index has value that falls between the refractive indices of core and cladding. This gave rise to a misconception that refractive index is a kind of weighted average of the refractive index of core and cladding of the waveguide. The weight factors are determined by the fractions of optical power propagating in core and cladding. Consider a step-index multimode fiber with high numerical aperture (NA), i.e. with a very large index step. In that case, all fiber modes propagate basically only in the core with the exception of the higher order ones. This might lead us to believe the effective index of all modes to closely match the core index. But on the contrary, higher-order modes still have significantly lower effective indices. They experience a smaller phase shift per unit length in spite of propagation through the same material.

Essentially it is the fact that higher-order modes contain more pronounced plane wave components (spatial Fourier components) with a larger angular offset from the fiber axis. So in a sense it is a matter of different propagation directions and not of different materials. However, both the effects become relevant in case of fibers having lower NA [50]. For multimode waveguides, the effective refractive index depends not only on the wavelength but also on the mode of light propagation. So, it is also called modal index. Obviously, the effective index is not just a material property, it depends on the whole waveguide design too.

3.4. Effective Area

The effective area can be defined as a quantitative measure of the area which a waveguide effectively covers in the transverse dimensions. All nonlinear effects depend upon the intensity of the electromagnetic field in the medium. However, it is the total optical power entering and leaving the fiber that is usually measured [51]. The measured optical power leaving a fiber is simply the integral of the electromagnetic field over the entire fiber cross section. The electromagnetic field is given by,

$$E = \sqrt{{E_x}^2 + {E_y}^2} \quad (3.5)$$

Where E_x is the x-component of electric field and E_y is the y-component of electric field. The effective area is defined as,

$$A_{eff} = \frac{\iint (|E|^2 dxdy)^2}{\iint |E|^4 dxdy} \tag{3.6}$$

Normalized effective area can be expressed as,

$$A = \frac{A_{eff}}{R^2} \tag{3.7}$$

However, often the normalized effective area can be more significant or useful. The fundamental mode being confined in the core possesses a lower normalized effective area compared to the higher order modes. The field in a single mode fiber is not evenly distributed or even fully contained within the core. It is larger at the fiber axis than near the core-cladding interface and extends into the cladding to a degree depending on the actual refractive index profile. In our work, the effective area has been calculated corresponding to both the core and the cladding area, because the field distribution is not uniform and hence is a non-vanishing part of the propagation in the cladding region of the fiber.

3.5. Confinement Factor

The confinement factor can be defined as the fraction of the total power residing in the silicon core. In our work, the power has been calculated from the pointing vector using all six component of the electric and magnetic fields [28]. Confinement factor can be expressed by the equation,

$$C_f = \frac{P_c}{P_o} \tag{3.8}$$

where is P_c the power confined in core and P_o is the total power confined in fiber.
Confinement refers to the amount of the core which is doped. Fiber core fabricate doped fibers have uniform doping across the core, so confinement factor in this case is unity. Some fiber designs have only part of the core doped [52].

3.6. Modal Hybridness

Waveguide with two-dimensional confinement are not strictly TE or TM, but hybrid in nature, which means that all the six components of the vector magnetic and electric fields are always present. For the fundamental quasi-TE (H_{11}^{y}) mode, the H_y component is dominant and the nondominant $H_x$component is often very small. Similarly, for the

fundamental quasi-TM (H_{11}^{x}) mode its component H_x is the dominant and the H_y component is nondominant. The hybridness of an optical mode may be defined as the ratio of the non-dominant to the dominant transverse components. As an example, for the quasi-TE modes (or H_{mn}^{y}), this is given by H_x/H_y. Similarly, for the quasi-TM modes (or H_{mn}^{x}), the hybridness is given by the H_y/H_x ratio, H_y being the non-dominant transverse component.

The hybridness of a mode increases when the index contrast Δn is increased such as in a semiconductor waveguide, or as the mode approaches its modal cutoff. It has also been shown that the hybridness increases significantly when the symmetry of a waveguide is broken or when the two orthogonally polarized modes are degenerate, i.e. they have nearly identical propagation constants (β). The hybridness of the guided modes can play an important role in the design of all the semiconductor optoelectronic systems. This effect can cause significant performance deterioration by introducing undesirable polarization cross-talk. To study modal hybridness it is essential to consider a fully vectorial modal solution approach. In this study, the $\vec{H}$ field based variational formulation is used, which is considered to be one of the most appropriate approach for optical waveguides, since all three components of the magnetic field are naturally continuous across the dielectric interfaces, unlike its dual $\vec{E}$ field based formulation.

3.7. Sellmeier Equation

Sellmeier formula is widely used in optical science and optical industry to describe and Characterize the dispersion in glasses and crystals. It is used in specification of wave dependent refractive index of a transparent material.

The usual form of Sellmeier equation is [53]

$$n(\lambda) = \sqrt{1 + \sum_{i=0}^{n} A_i \frac{\lambda^2}{\lambda^2 - \lambda_i^2}} \tag{3.9}$$

Here $n(\lambda)$ is the refractive index for wavelength λ. A_i and λ_i are known as Sellmeier co-efficient. For i= 3 Eq. 1 was named 3-term Sellmeier equation. That means measuring the refractive index of the medium at least at 6 different wavelengths we are able to calculate 6 Sellmeier co-efficient A_1, A_2, A_3, λ_1, λ_2 and λ_3 and to approximate the dispersion curve. For fused silica (SiO_2) [54]:

$$n^2 - 1 = \frac{.6961663\lambda^2}{\lambda^2-(.0684043)^2} + \frac{.4079426\lambda^2}{\lambda^2-(.1162414)^2} + \frac{.8974794\lambda^2}{\lambda^2-(9.896161)^2} \quad (3.10)$$

For single crystal silicon [55]:

$$n^2 = 11.6858 + \frac{.93816}{\lambda^2} + \frac{.000993358}{\lambda^2-1.22567} \quad (3.11)$$

Where the unit of λ is μm.

Table 3.2: Sellmeier coefficients of glasses with different dopants [53]

Material	A_1	λ_1	A_2	λ_2	A_3	λ_3
SiO_2	0.696750	0.069066	0.408218	0.115662	0.890815	9.900559
13.5% GeO_2 + 86.5% SiO_2	0.711040	0.064270	0.451885	0.129408	0.704048	9.425478
9.1% P_2O_5 + 90.9% SiO_2	0.695790	0.061568	0.452497	0.119921	0.712513	8.656641
13.3% B_2O_3 + 86.7% SiO_2	0.690618	0.061900	0.401996	0.123662	0.898817	9.098960
1% F + 99% SiO_2	0.691116	0.068227	0.399166	0.116460	0.890423	9.993707

3.8. Nonlinearity

The terms linear and nonlinear in optics, mean intensity independent and intensity-dependent phenomena respectively. When the output signal strength does not vary in direct proportion to the input signal strength, then it is called the nonlinearity of the device. For a nonlinear device the output-to-input amplitude ratio (also called gain) depend on the strength on the strength of the input signal [56]. Nonlinear effects in optical fibers occur due to,

(1) Change in the refractive index of the medium with optical intensity and,
(2) Inelastic scattering phenomenon.

For optical fibers, even moderate optical power leads to high optical intensities because of the light is confined to a small transverse region. In addition, light often propagates over considerable distances in fiber optic. For these reasons, nonlinear effects to fiber

nonlinearities often have substantial effect [57].

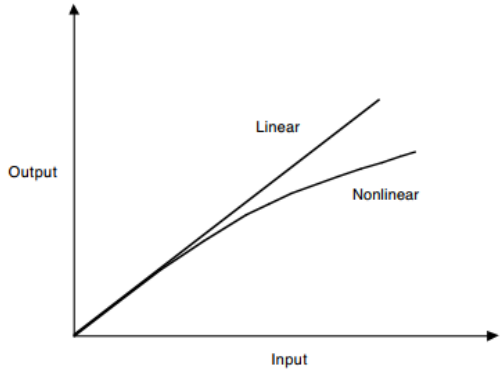

Fig.3.5. linear and nonlinear interaction

The power dependence of the refractive index is responsible for the Kerr-effect. This is the most common nonlinear effects in fiber. Certainly, this means that the phase delay in the fiber gets larger if the optical intensity increases. This can be described via an increase of refractive index in proportion to the intensity,

$$\Delta n = n_2 l \tag{3.12}$$

That increase can often be considered as instantaneous, even though this is not exactly true in reality. The nonlinear index n is rather small for silica fibers around 2.3×10^{-20} m^2/W for wavelengths around 1.5 μm. Depending upon the type of input signal, the Kerr-nonlinearity manifests itself in three different effects such as Self-Phase Modulation (SPM), Cross-Phase Modulation (CPM) and Four-Wave Mixing (FWM). At high power level, the inelastic scattering phenomenon can induce stimulated effects such as Stimulated Brillouin-Scattering (SBS) and Stimulated Raman-Scattering (SRS).

Self phase modulation is one of the consequences of Kerr effect that is shown in refractive index. This means that a light wave in the fiber experiences a nonlinear phase delay which results from its own intensity. For a fiber mode, the phase change per unit optical power and unit length is described by the proportionality constant γ (in unit of rad /(W·m)),

$$\gamma = \frac{2\pi n_2}{\lambda A_{eff}} \tag{3.13}$$

Where the value of n_2 is 2.3×10^{-20} m^2/W and A_{eff} is effective area. If an optical pulse is transmitted through a fiber, the kerr effect causes a time dependent phase shift

according to the time dependent pulse intensity. The overall effect of Kerr nonlinearity and dispersion is strongly dependent on the dispersion properties. Most nonlinear effects can be reduced by using a fiber with a large effective mode area, as this leads to lower optical intensities for a given power level. This is essentially because larger modes are more sensitive to lensing effects. As a result, the optical peak power in a fiber must always be limited to a few megawatt.

Nonlinear effects such as SPM, CPM, and FWM are discussed. These effects degrade the performance of fiber optic systems. Impact of SPM is negligible if power per channel is below 19.6 mW. Nonlinearity can be tolerated in devices and systems that use digital modulation, and also in frequency modulation (FM) wireless transmitters. These signals are either full-on or full-off; the amplitudes waveforms are not analog, so analog distortion cannot occur. In analog devices and systems, however, linearity is important. Nonlinear circuits generally cause distortion in applications such as amplitude-modulation (AM) wireless transmission and hi-fi audio.

3.9. Dispersion

Dispersion is the spreading out of a light pulse in time as it propagates down the fiber. It is measured in pulse broadening in time over a unit length of fiber (i.e. $ns.km^{-1}$). Spectral components of a pulse propagating down an optical fiber reach their destination at slightly different times. This translates into a wider pulse at the receiving end of the fiber. Dispersion affects the bandwidth of the system, hence maintaining low dispersion is of equal importance for ensuring increased system information capacity, versatility and cost effectiveness.

3.9.1. Dispersion in single-mode fibers

Dispersion in single-mode fibers is an intramodal effect and is a result of group velocity dependence on wavelength. Because of that, the amount of signal distortion depends on the spectral width of the optical source used. Three mechanisms contribute to intra modal dispersion:

- Material dispersion,
- Waveguide dispersion and
- Polarization-mode dispersion.

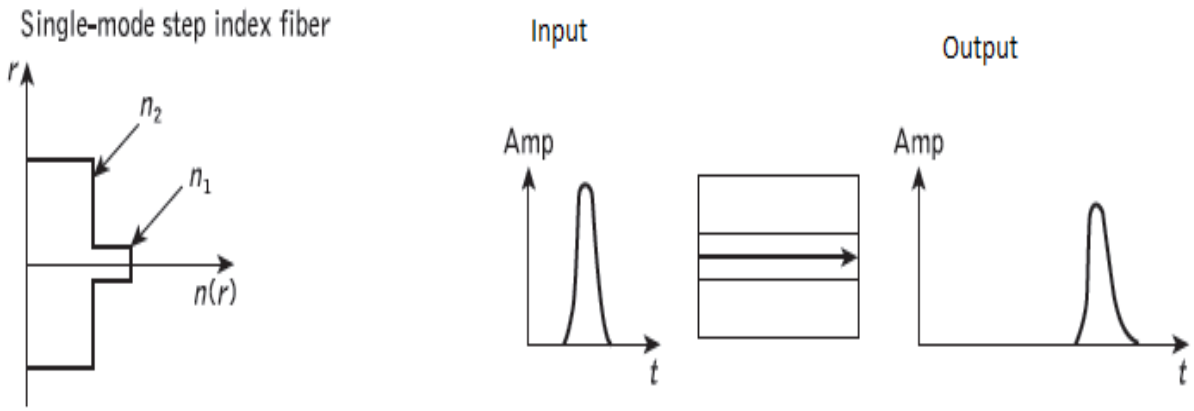

Fig. 3.6. Dispersion in Single mode fiber [23]

Material dispersion

It is also known as spectral or chromatic dispersion. Material dispersion is caused by nonlinear variations of refractive index of the fiber material with respect to wavelength. Since the phase velocity is a function of the refractive index, the spectral components of any given signal will travel at different speeds which cause deformation of the pulse. A material is said to exhibit material dispersion when the second differential of the

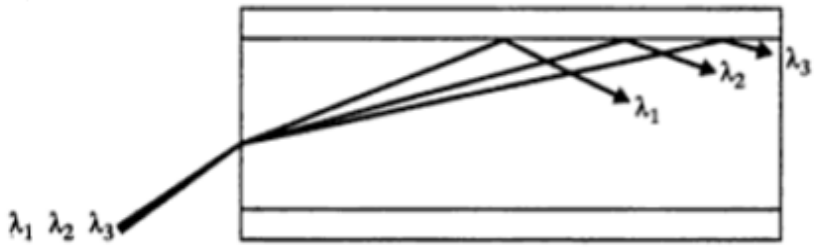

Fig.3.7: Material Dispersion [58].

refractive index with respect to wavelength is not zero ($d^2n_{eff}/d\lambda^2 \neq 0$).The co-efficient of Material dispersion is *D* (in unit of ps/Km/nm) is [23]:

$$\mathrm{D} = -\frac{\lambda}{c}\frac{d^2 n_{eff}}{d\lambda^2} \tag{3.14}$$

Waveguide dispersion

Waveguide dispersion is only important in single mode fibers. It is caused by the fact that some light travels in the fiber cladding compared to most light travels in the fiber core. Since fiber cladding has lower refractive index than fiber core, light ray that travels in the cladding travels faster than that in the core. Waveguide dispersion is also a type of chromatic dispersion. It is a function of fiber core size, V-number, wavelength

and light source linewidth. It is the result of axial propagation constant β being a function of wavelength ($d^2\beta/d\lambda^2 \neq 0$) due to the existence of one or more boundaries in the structure of the fiber. Without such boundaries, the fiber reduces to a homogeneous medium, the fundamental mode becomes a uniform plane-wave, and the waveguide dispersion effect is eliminated. In multimode fibers, where the majority of modes propagate far from cutoff, are almost free of waveguide dispersion and it is generally negligible compared with material dispersion.

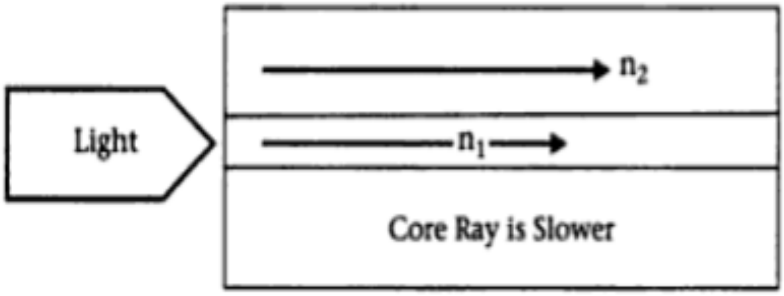

Fig.3.8. Waveguide Dispersion [58].

Polarized dispersion

Single-mode fibers, in reality, support two orthogonally-polarized fundamental modes. In perfectly circular fibers, these two modes have identical propagation constants and pulse spreading due to polarization-mode dispersion does not exist. In practical fibers, there is a small difference between the propagation constants of these two modes due

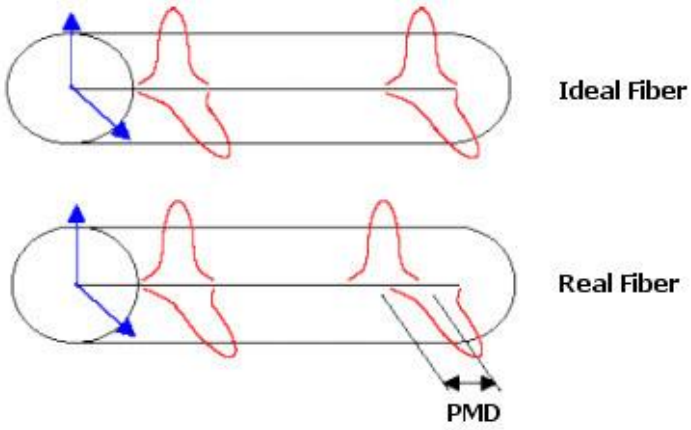

Fig. 3.9 Polarization Mode Fiber [59].

due to the slight ellipticity of the core. The presence of two fundamental modes contributes to pulse spreading. This phenomenon is known as polarization-mode dispersion.

3.9.2. Dispersion in multimode fibers

In applications where two or more modes travel simultaneously though the fiber, intermodal as well as intramodal dispersions exist. Intermodal dispersion does not occur in single-mode fibers, but is a significant effect in multimode fibers. It occurs as a result of different modes having different group velocities at the same frequency.

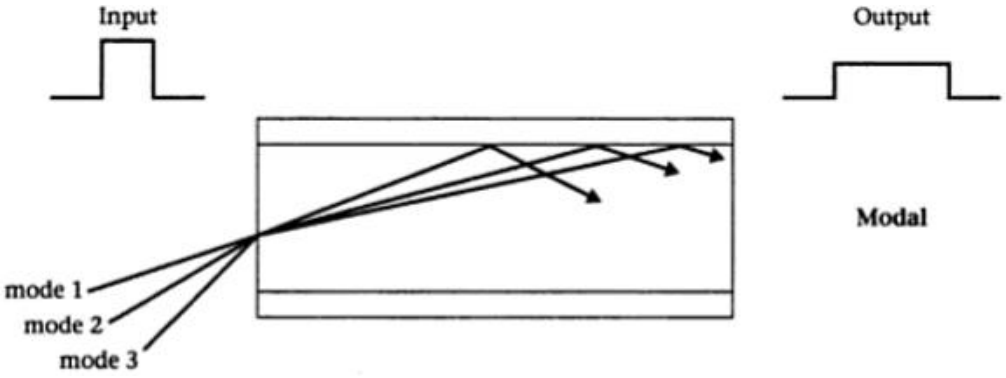

Fig. 3.10. Intramodal Dispersion [58].

Graded-index fibers with nearly parabolic-index profile were developed mainly to reduce the effect of intermodal dispersion. Here, bound rays deviating from the axis of the fiber travel a longer distance but at larger velocities, reaching the receiving end of the fiber at about the same time with the other rays, thus in graded-index fibers pulse spreading is significantly reduced. Although all forms of dispersion present in single-mode fibers exist in multimode fibers too, material dispersion is the only significant intramodal effect which should be considered. Thus, pulse spreading in multimode fibers is largely due to material dispersion and intermodal delay distortion.

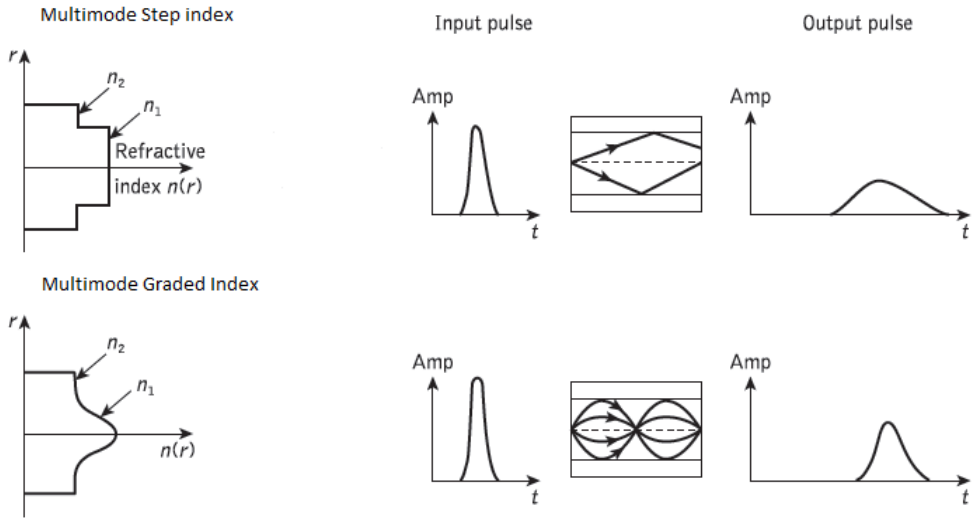

Fig.3.11: Dispersion in multimode fiber [23].

CHAPTER 4

ANANLYSIS OF SILICON AND SILICA NANOWIRE

The results obtained after simulation of the designed nanowires are represented in this chapter. And later on the results for Silica nanowire as optical sensor was shown. Nanowire is designed following the process that has been explained in chapter 2.

4.1. Silicon Nanowire

4.1.1. Different Optical Modes

In this chapter different modes of Silicon nanowire with silica cladding have been studied, where η_{core}=3.4754 and η_{clad} =1.444 at 1.55 μm wavelength for core radius r_{core}= 1.4 μm. For the nomenclature LP_{mn} was used where m and n represent mode orders in azimuthal and radial directions respectively. The modes are dominated by either H_x or H_y field. Modes are classified as x-polarized or y- polarized where x-polarized mode is with dominant H_y and E_x field and y-polarized mode is with dominant H_x and E_y field. The H_{mn}^x and H_{mn}^y notation is used here which is identical to that of the LP_{mn} modes. Dominant H-field component is identified by H_x or H_y. All the studies here have been considered with dominant H_x field if not mentioned otherwise. Only a finite number of guided propagation modes are seen in a Silicon nanowire waveguide and the intensity distribution of which have a finite extent around the waveguide core. The waveguide structure and optical frequency in very important in this case. Because the number of guided modes, their transverse amplitude profiles and their propagation constants depend on the details of waveguide structure and optical frequency. Fig. 4.1 and Fig. 4.2 show different modes for magnetic field x component. The electric field of H_{01}^x mode of x, y, z-component are shown in Fig. 4.3 (a), (b), and (c). Fig. 4.4 (a) shows the 3-D diagram of the magnetic field (H_{01}^x mode) for R=1.4 μm. For the same core radius the vector plot of magnetic field and electric field of H_{01}^x mode and the contour plot of the magnetic field (H_{01}^x mode) are shown in Fig. 4.4 (b) and (c) in that order. Fig. 4.5 illustrates the average power flow of mode of z-component.

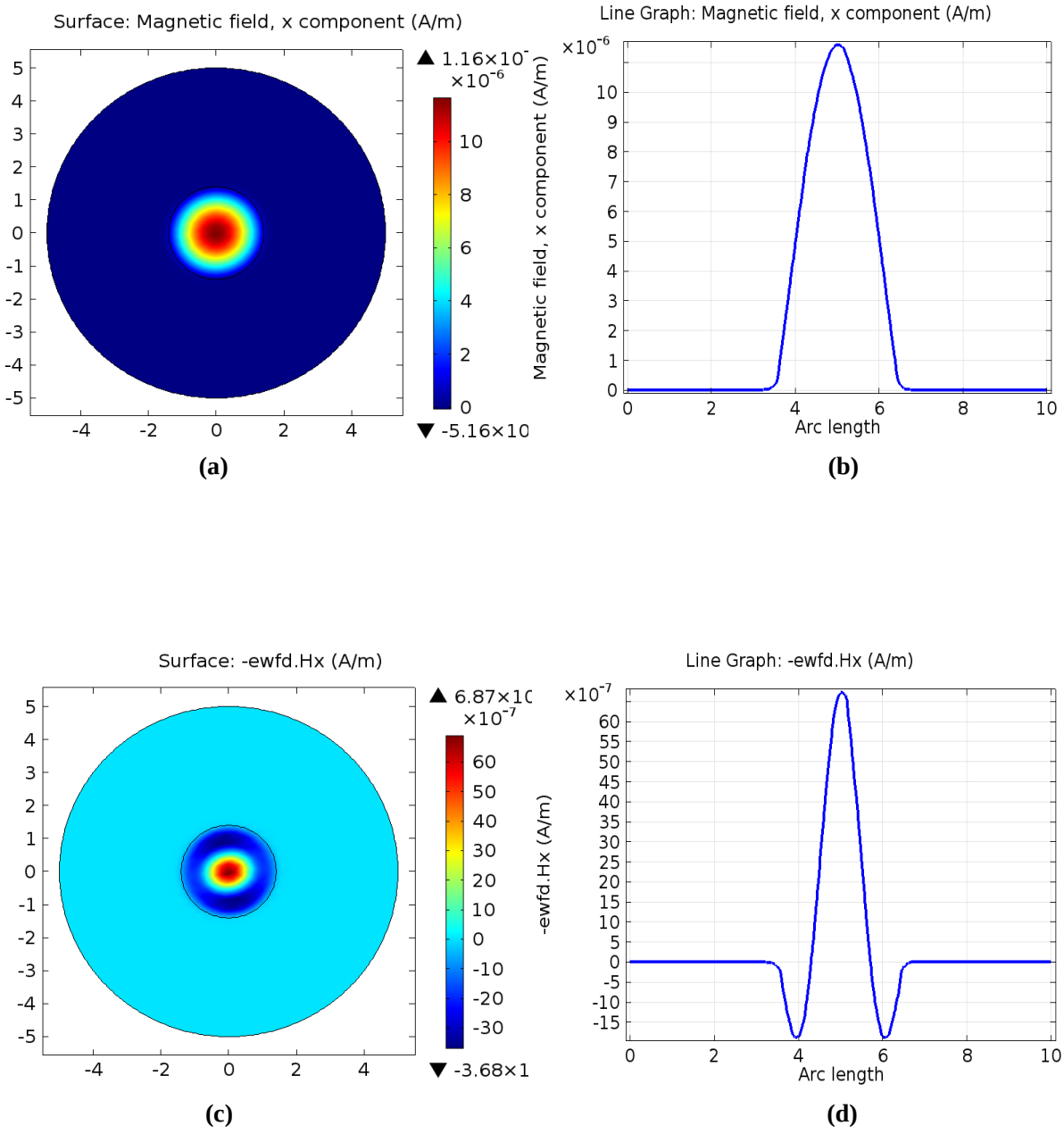

Fig. 4.1: For R=1.4 µm (a) magnetic field of H_{01}^{x} mode, (b) line graph of the magnetic field of H_{01}^{x} mode, (c) magnetic field of H_{02}^{x} mode, (b) line graph of H_{02}^{x} mode.

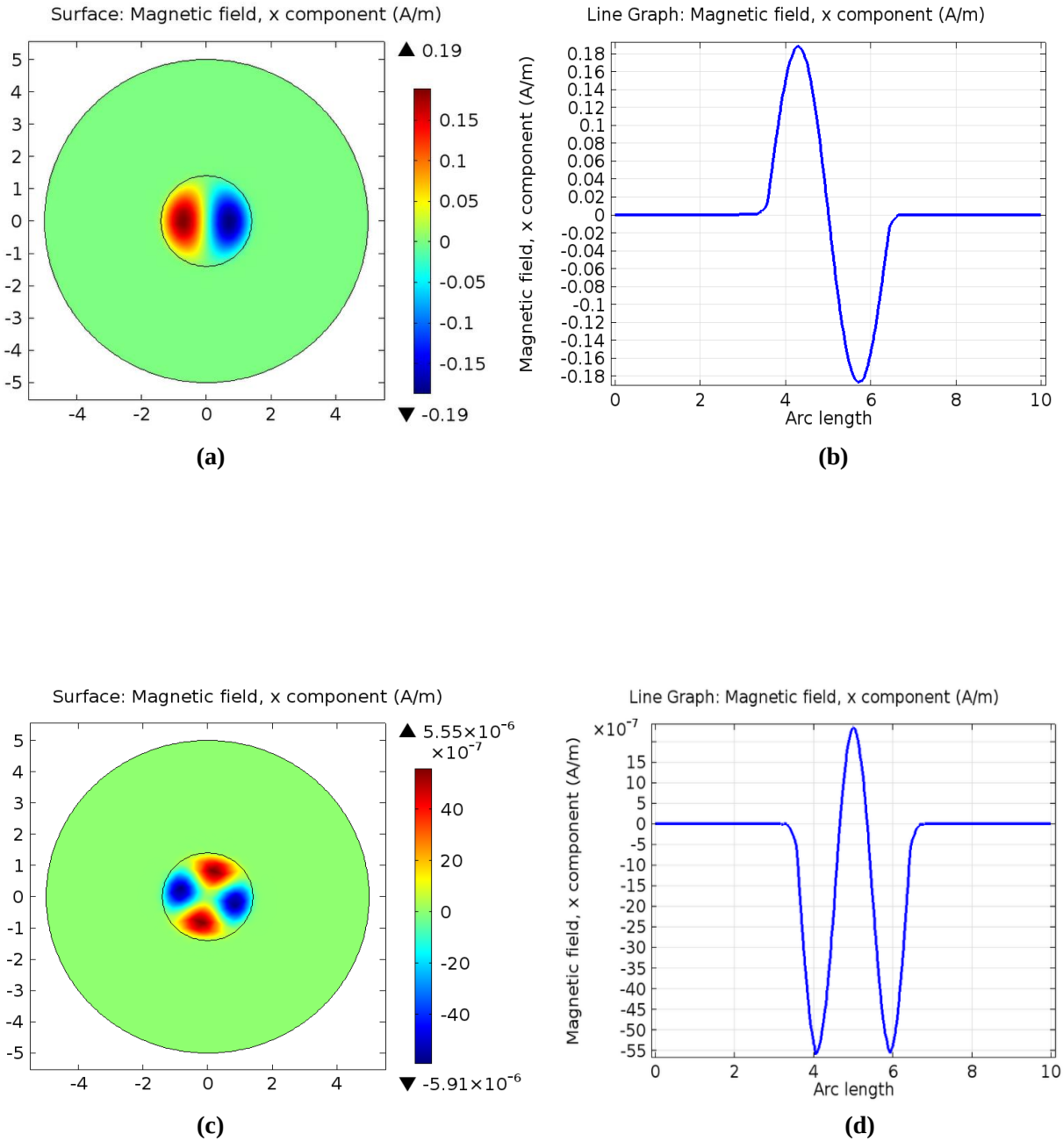

Fig. 4.2: For R=1.4 µm (a) magnetic field of H_{11}^{x} mode, (b) line graph of the magnetic field of H_{11}^{x}mode, (c) magnetic field of H_{21}^{x} mode, (b) line graph of H_{21}^{x} mode.

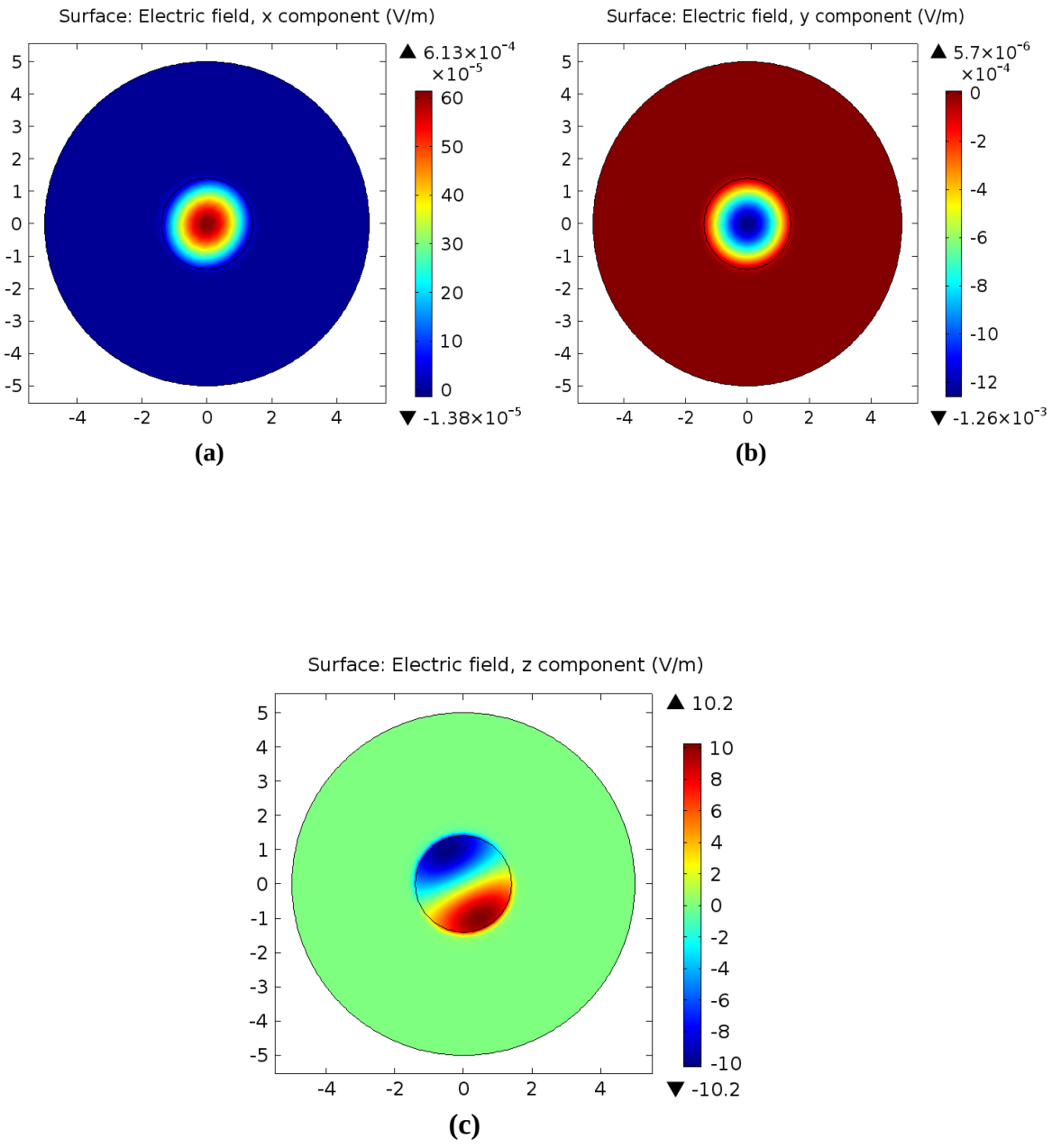

Fig. 4.3: The electric field of H_{01}^{x} mode of (a) x-component, (b) y-component, and (c) z-component.

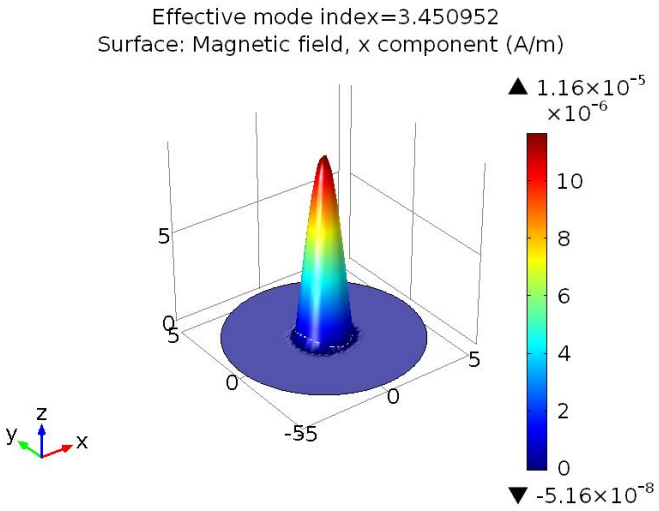

(a)

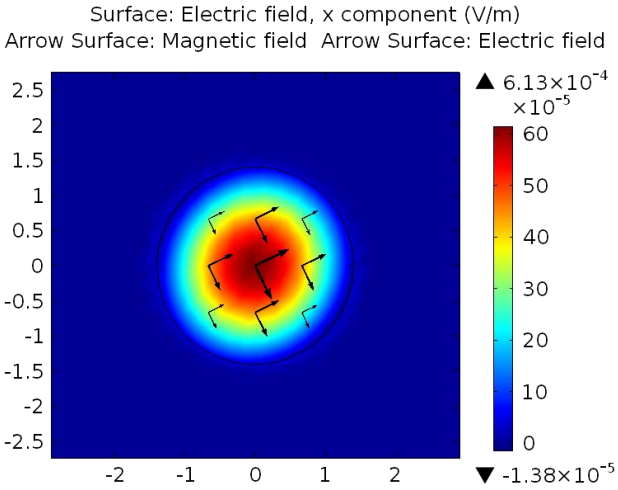

(b)

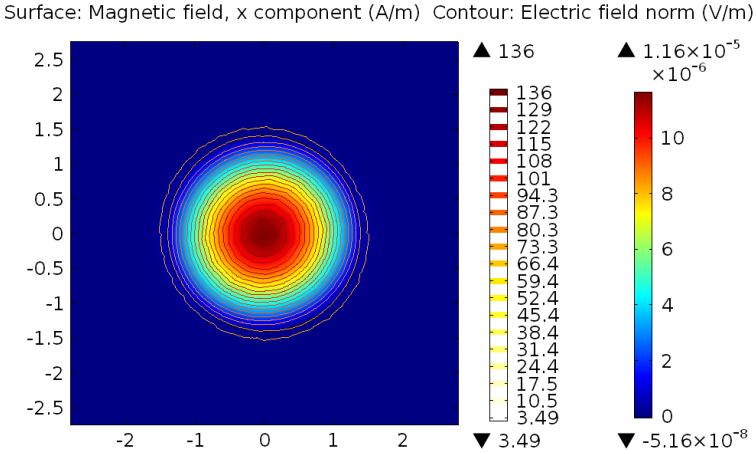

(c)

Fig. 4.4: For R=1.4 µm of mode H_{01}^{x} (a) 3-D diagram of the magnetic field, (b) vector plot of magnetic field and electric, and (c) contour plot of the magnetic field.

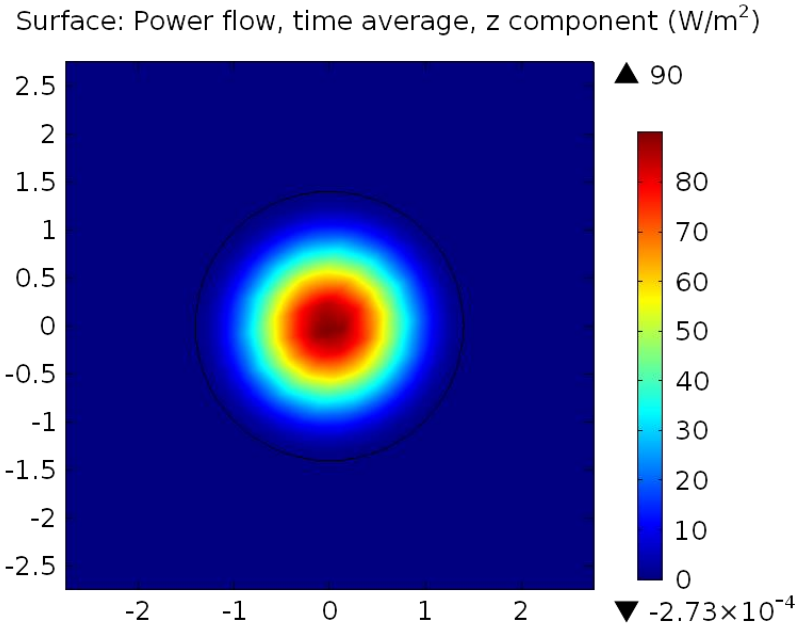

Fig. 4.5: Average power flow of H_{01}^{x} mode of z-component.

4.2. Characteristics of Silicon Nanowire

The properties which have been observed for the nanowire composed of Silicon core and Silica Cladding are briefly described here.

4.2.1. Effective index

In this thesis work, Silicon core of radius R with a circular geometry has been scrutinized, with a Silica cladding. Fig. 4.6 shows the variation of effective indices for a Silica circular optical waveguide as the radius is reduced and enters the nanowire regime. For the fundamental mode H_{01}^{x} variation in effective index with respect to radius is observed in Fig. 4.6 where effective index η_{eff} satisfies (3.2). Since the quasi-TM and TE fundamental H_{01}^{x} and H_{01}^{y} of the waveguide are degenerate for the circular optical waveguide the effective indices of H_{01}^{y} are not shown here. The higher order modes H_{11}^{x} (HE_{01} or LP_{11}), H_{21}^{x} (HE_{11} or LP_{21}) and H_{02}^{x} (HE_{21} or LP_{02}) [28] are also shown in Fig. 4.6. It is observed that at first the effective indices of the modes decreases slowly with decreasing core radius but as the modes approach their cut-off conditions these reduce rapidly. It can also be noted that when the radius is increased the effective index asymptotically approaches that of the Si and then most of the optical power is confined in the Si core.

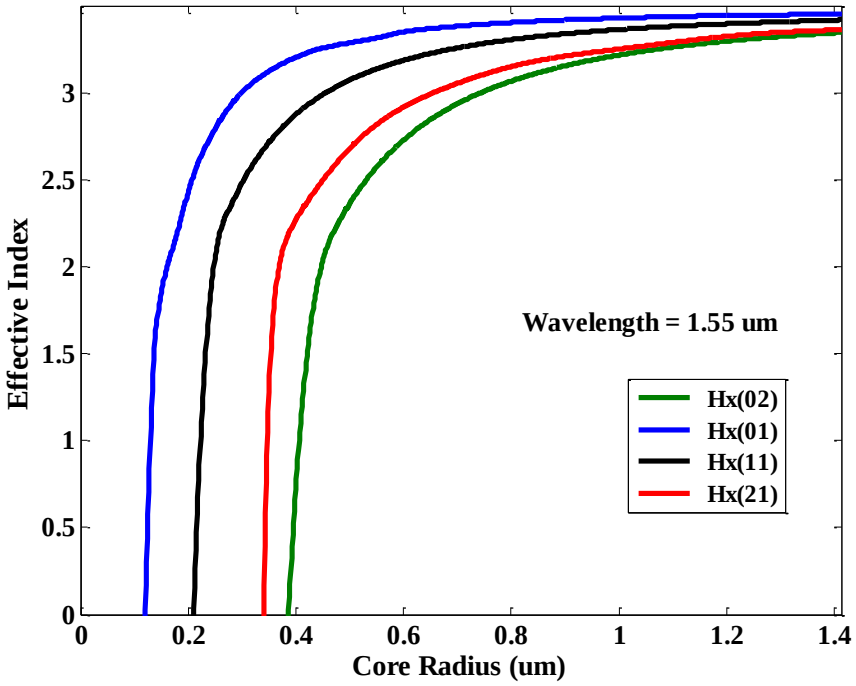

Fig. 4.6: Variations in the effective indices with the core radius.

4.2.2. Effective area

Fig. 4.7 shows the normalized effective area for different modes with respect to core radius (μm). Here the effective area and the normalized effective area can be calculated for equation (3.4) and (3.5) respectively.

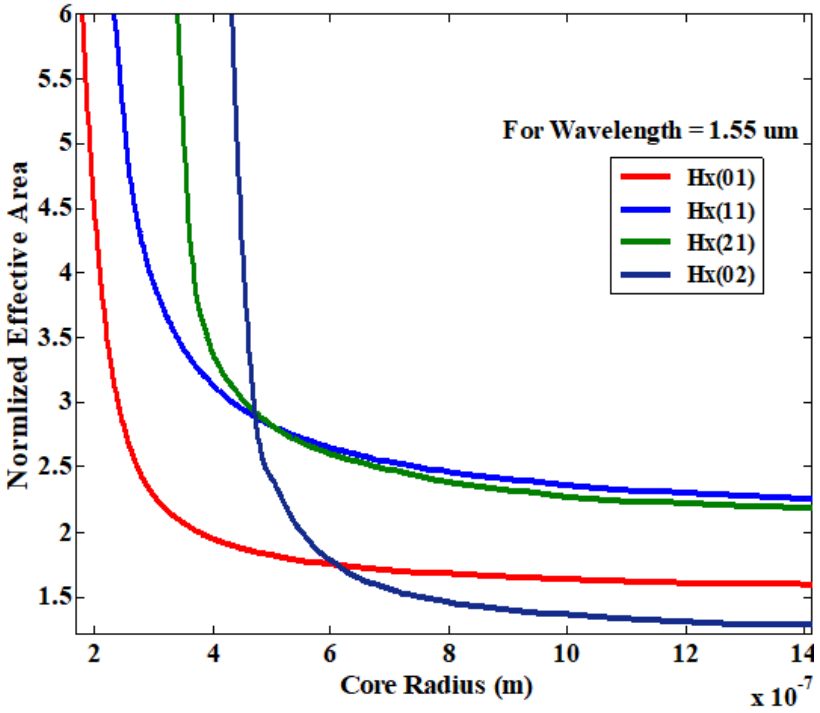

Fig. 4.7: Normalized effective area (A_{eff}) with core radius, R (μm) for various mode.

The fundamental mode possesses a lower normalized effective area compared to the higher order modes, as this mode is more confined to the core. As the core radius is reduced, the corresponding normalized effective area increases slightly until the mode approaches the cut off region. With the further reduction in R, the value of effective area increases rapidly, as the mode spreads into the cladding region. The normalized effective areas for the H_{02}^{x}, H_{11}^{x}, H_{21}^{x} and modes increase as they approach their cutoff region. It is observed from Fig. 4.14 that the mode has a lower normalized effective area for higher core radius but it approaches the cutoff condition before H_{11}^{x} and H_{21}^{x} modes when core radius is reduced.

4.2.3. Confinement factor

The optical confinement factor is defined as the proportion of the square of the electric field in the active region. It was often used in the analysis of vertical cavity surface-emitting. The confinement factor for Si is defined as the fraction of the total power residing in the Silicon core. The comparison of the confinement factor with the core radius for fundamental mode and higher order modes is shown in Fig. 4.8. Confinement factor is derived from (3.7).

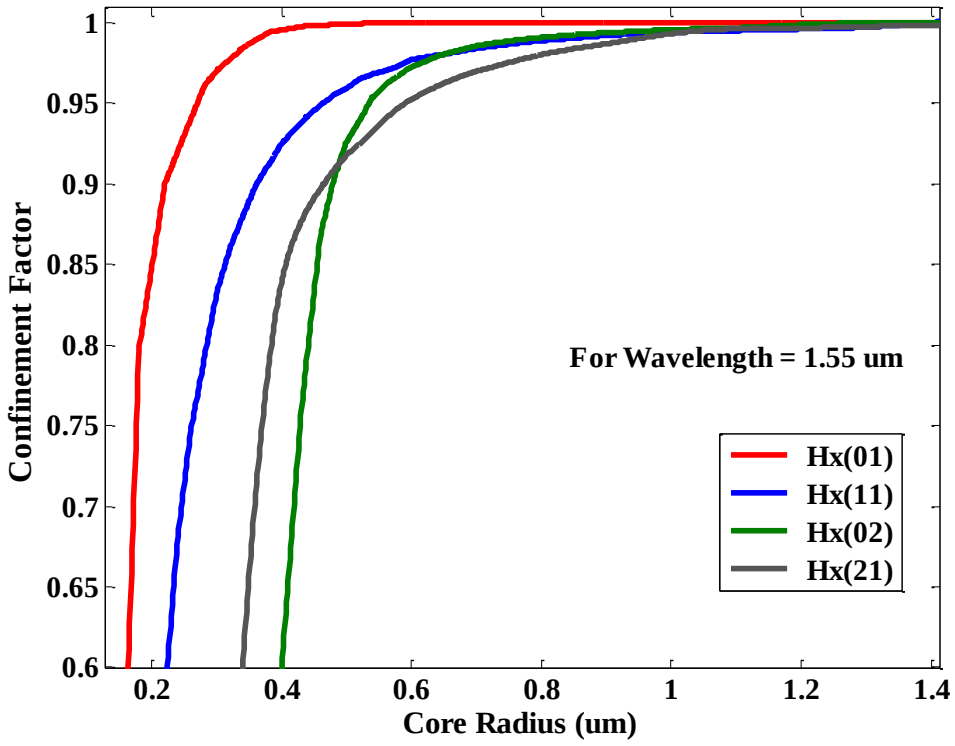

Fig. 4.8: Variations of the confinement factors for the fundamental and higher order modes with core radius, R (μm).

In this case, the power has been calculated from the Poynting vector using all six components of the E and H fields. From the graph it can be observed that the fundamental mode is near the cutoff region by the rapid increase in normalized effective area and rapid decrease in confinement factor beneath R=200 nm. From Fig. 4.8 It can also be observed that the cutoff radii for the H_{01}^{x}, H_{11}^{x}, H_{21}^{x} and H_{02}^{x} modes are approximately 160, 210, 340 and 410 nm respectively and these values also comply with the values obtained from Fig. 4.6. It is also observed from Fig. 4.8 that the H_{02}^{x} mode has a higher confinement factor (and lower normalized effective area) for higher core radius but it reduces faster than the H_{11}^{x} and H_{21}^{x} modes when core radius is reduced.

4.2.4. H-field mode profile

It has been observed that when the radius of the core R, is much smaller than the wavelength size, the fundamental mode may not be circular in shape, even though the nanowire structure is rotationally symmetric. The x component of the H field is dominant for the H_{01}^{x} mode and the H_x field is shown in Fig.4.9 where core radius, R=200 nm. It can be observed that the maximum field intensity is at the center of the core and decreases along the radial direction. Fig. 4.9(a) shows that the mode shape is not circular rather it is dumbbell-shaped due to the spreading of H_x field in the horizontal direction. Though the H_x field is dominant for the H_{01}^{x} mode the other two components are also present. Fig. 4.9(b) shows the H_y field which has four peaks with alternate positive and negative signs. Though its magnitude is smaller than the dominant H_x field, it is not trivial. Fig. 4.9(c) shows the H_z field from which it can be noted that it has two peaks along the X axis and its value along the Y axis is zero. For the fundamental H_{01}^{x} mode, the magnetic and electric wall boundary conditions exist along the Y and X axes respectively. Thus, even though the Hy field exists, its value is zero along both the axes. Fig. 4.10 shows the variation of H_x and H_z field along the axe, when R=200nm. For fundamental H_{01}^{x} mode, the boundary condition for magnetic and electric field exists along the Y and X axes respectively. For this mode H_y field exists but its value is zero along the X and Y axes, which is not shown here. Similarly the value of H_z is zero along the Y axis but nonzero along the X axis. From Fig. 4.13 it can be observed that the H_x field varies more slowly along the X axis and the variations of the H_x field along the Y axis almost identical for all the values of R.

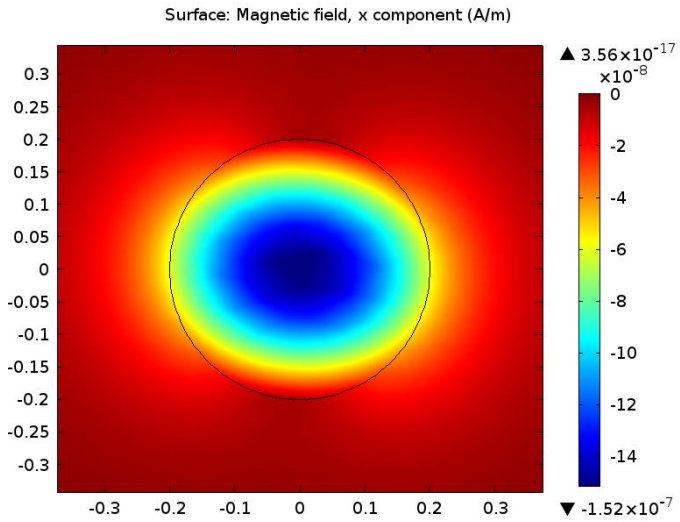

(a)

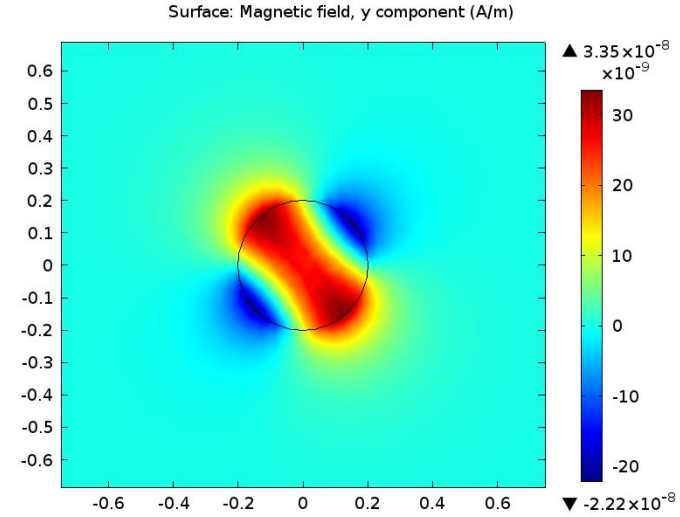

(b)

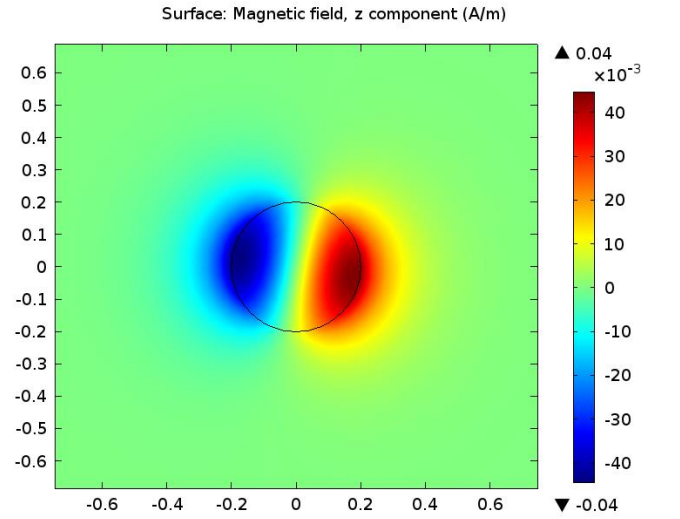

(c)

Fig. 4.9: (a) H_x field, (b) H_y field and (c) H_z field for the quasi H_{01}^x mode with core radius, R=200 nm.

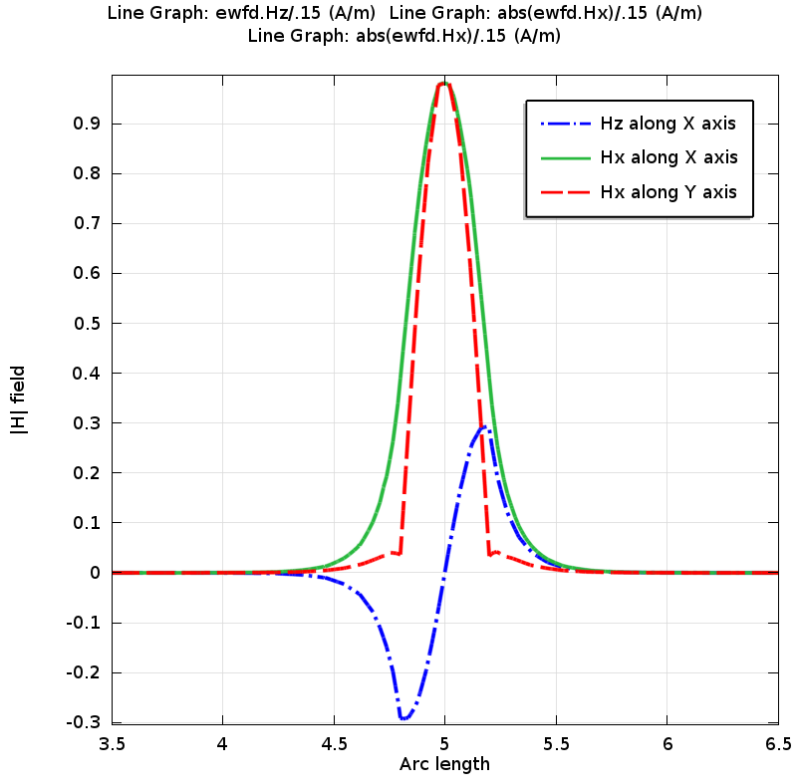

Fig. 4.10: Variation of the H fields along the X and Y axes for the quasi H_{01}^{x} mode.

It is also observed that the maximum value of H_z field is about 30% of the maximum H_x value. The variation of dominant H_x field profile is not identical in the direction of X and Y axes because of boundary conditions for the H_x field component which leads to an elliptical profile of the H_x field for the fundamental H_{01}^{x} mode.

4.2.5. E-field mode profile

Once the magnetic field, H, is obtained from this H-field formulation, the corresponding E-field can be calculated from ∇×H Maxwell's equations. For the mode of H_{mn}^{x}, the E_y field is dominant and directly related to the H_x field with an additional contribution from $\frac{\delta H_z}{\delta x}$. The variation of electric field E_y component along X and Y axes are shown in Fig. 4.11. From Fig. 4.11 it is observed that E_y field is continuous along the X axis as E_y is tangent to the core at x=R but discontinuous along Y axis because E_y field in normal to the interface at y=R. Here it is also shown that variation of E-field along X and Y axes direction is not identical, which rise the asymmetry of the optical beam profile. From Fig. 4.10 H_y field is zero along X and Y axes so that E_x field is zero along the X and Y axes and is not shown in Fig. 4.11. E_z field variation along Y axis is shown

here when, R=200 nm. Along X axis the E_z field is zero because of the boundary condition of electric wall for mode H_{01}^{x}.

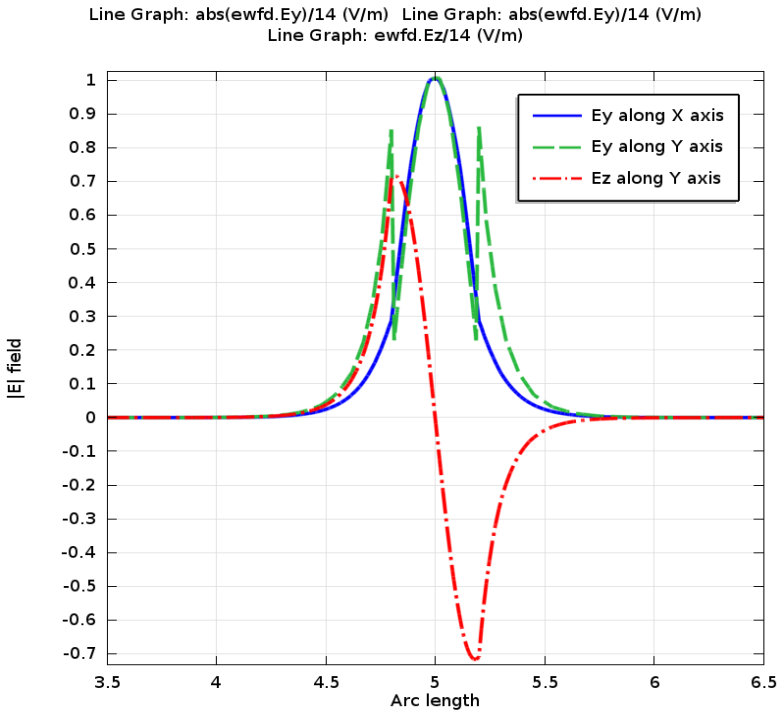

Fig. 4.11: Variation of E-fields along the X and Y axes for the quasi H_{01}^{x} mode.

4.2.6. Modal hybridness

For the H_{mn}^{x} mode, the hybridness can be defined as the ratio of the maximum values of the nondominant H_y or the H_z field over the dominant H_x field. Because of the presence of the nondominant component, the H_{mn}^{x} mode is a quasi-vertically polarized mode. The modal hybridness increases with the index contrast, and this can be enhanced further by the presence of waveguide asymmetry. In a low index contrast waveguide hybridness is very small. However, it is expected that hybridness would be higher in a high index contrast silicon nanowire. In Fig. 4.12 the variation of modal hybridness with respect to core radius is shown. In Fig. 4.12 the variation of modal hybridness with respect to core radius is shown. It can be observed that, as the core radius is much smaller than λ (=1.55 μm), the hybridness increases vary rapidly. At R= 400 nm, the modal hybridness reaches a value that is significantly higher compared to that when the core is as large as R = 1.4 μm. Modal hybridness is a key modal property in polarization issues such as polarization cross talk or polarization mode dispersion. Polarization conversion can take place due to the interaction of the dominant and nondominant components of the H_x^{01} and H_y^{01} modes [19], which this is an important parameter for

polarization cross talk studies.

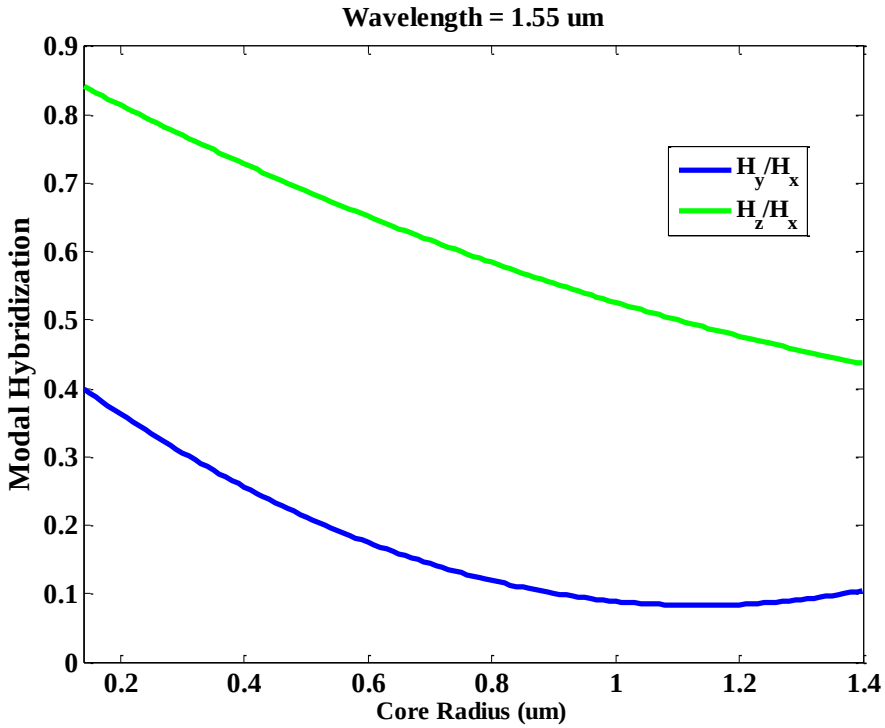

Fig. 4.12: Variation of the H_y/H_x and H_z/H_x with core radius, R for the quasi H_{01}^x mode.

4.2.7. Nonlinearity

Fig. 4.13 shows the evalution of nonlinearity with respect to the core radius for fundamental mobe and higher order modes. Nonlinearity is derived from equation (3.13). From the fig. 4.13 it can be said that the fundamental mode is near the cut off region by the decrease in nonlinearity beneath R=200nm. In the same way, it can also be noted from the cutoff radii for the H_{01}^x, H_{11}^x, H_{21}^x and H_{02}^x modes are approximately 160, 210, 340, and 410 nm respectively and these values also abide by with the values obtained from Fig. 4.1. From Fig. 4.14 it is also observed that the nonlinearity decreases for the H_{11}^x, H_{21}^x and H_{02}^x modes, as they approach their cutoff condition. One feature it can be noticed that the H_{02}^x mode has a higher nonlinearity (and lower normalized effective area) for higher core radius but it decreases gradually when core radius is reduced. And it rapidly decreases when core radius is near cutoff regime. For core radius R=800 nm, the nonlinearity profile with different wavelength for fundamental mode and higher order modes is observed in Fig.4.14. To obtain their wavelength dependent refractive index Sellmeier equations for silica and silicon have been used and the nonlinearity is derived from (3.13). It is observed that the nonlinearity increases as the decrease in wavelength for all mode of H_{01}^x, H_{11}^x, H_{21}^x and H_{02}^x. H_{02}^x mode has a

higher nonlinearity (and lower normalized effective area) for lower wavelength; this value reduces gradually as wavelength increases. It is noticed that when the wavelength is higher than 1.8 m, the nonlinearity decreases more compare to the other two modes: the H_{01}^{x} and H_{11}^{x} modes.

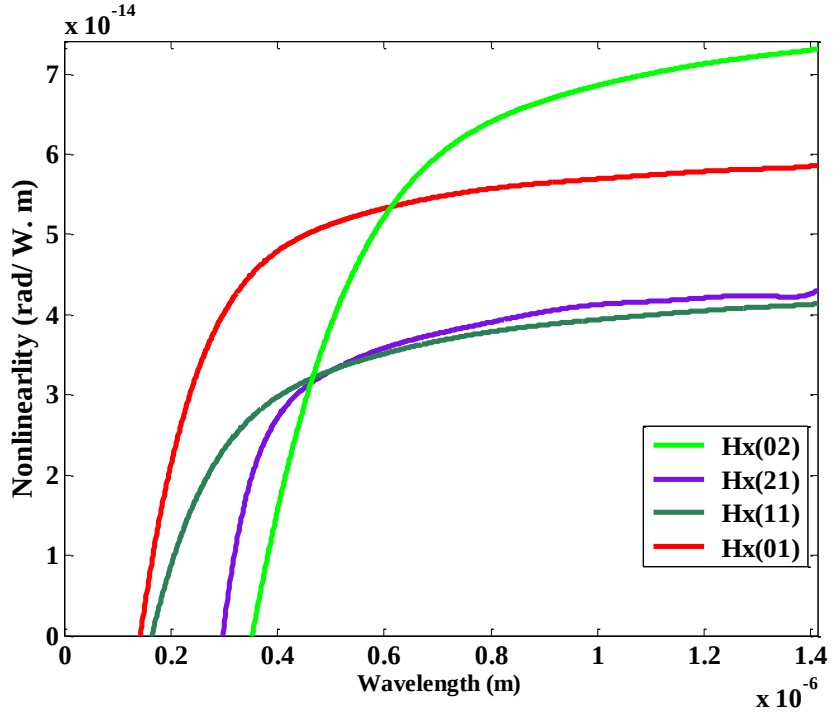

Fig. 4.13: The variation of the nonlinearity γ with the wavelength λ.

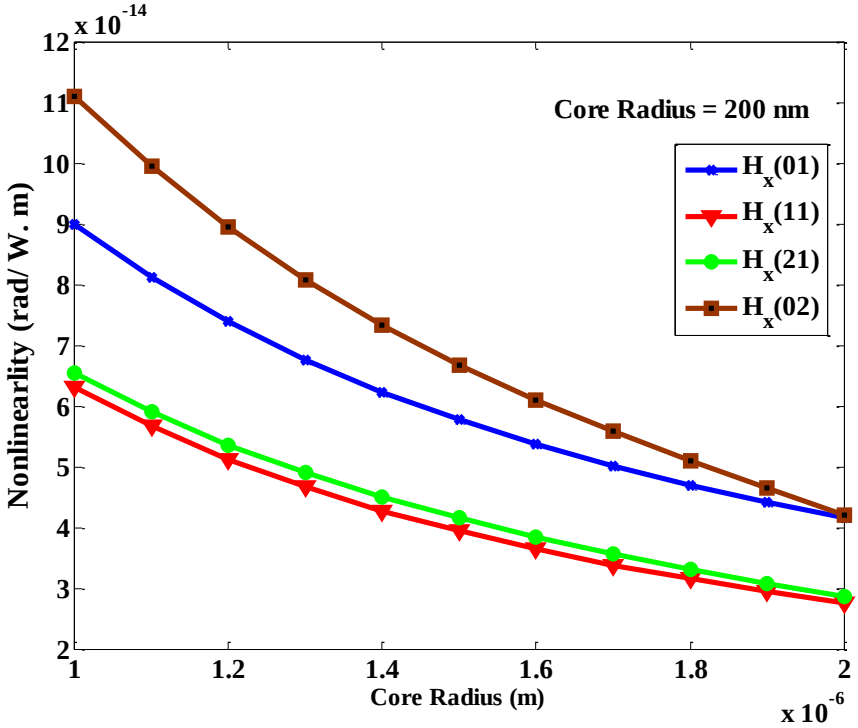

Fig. 4.14: The variation of the nonlinearity γ with the core radius.

4.2.8. Dispersion

Dispersion is the spreading out of a light pulse in time as it propagates down the fiber. Dispersion in optical fiber includes model dispersion, material dispersion and waveguide dispersion. The dispersion profiles for five different core diameters have been shown in Fig. 4.15. Sellmeier equations for silica and silicon have been used to obtain their wavelength dependent refractive index values.

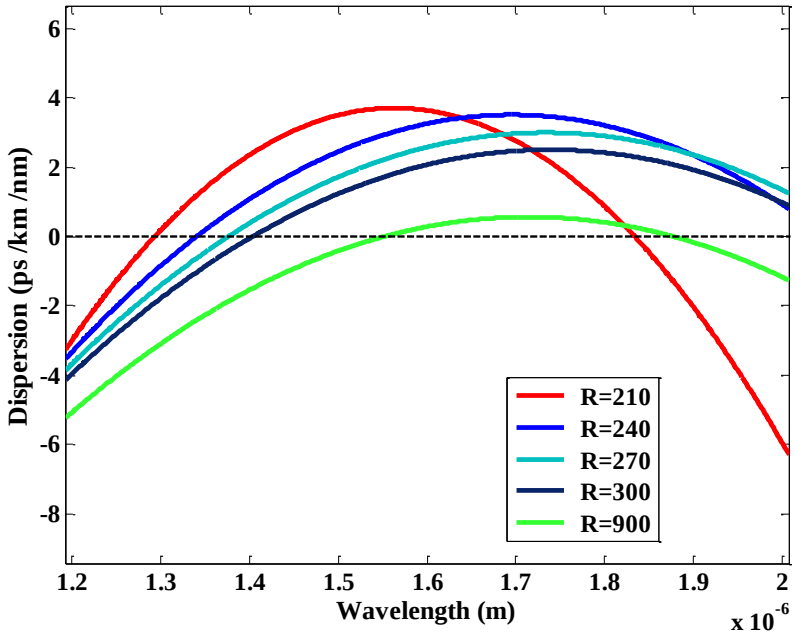

Fig 4.15: Dispersion with wavelength for five different core radius for silicon core with silica cladding

The GVD values, D, are found from equation (3.14). When core radius is as large as R=900nm, most of the power happen to reside inside the core with a confinement factor greater than about 0.99, hence dispersion curve is nearly analogous to the material dispersion of silicon. When radius R=300 nm, field remains confined in the silicon core for smaller wavelength. Further increase of wavelength significantly spreads the modal field into the cladding resulting in the profile deviating from the circular shape. With the electric field starting to penetrate into the silica region, the effective index reduces at a faster rate with the increase of the wavelength. Consequently, a zero dispersion is seen around λ=1.41 μm for R=300 nm. The zero dispersion is blue shifted with the reduction of the core radius. The buildup of power in silica lean towards larger values for small core radius value, so that dispersion reaches the peak value at a particular higher wavelength. Afterwards further increase in the wavelength decreases the

effective index but now at a slower rate. This results in the change of slope in the higher wavelength region for smaller core radius as seen for R=210 nm – 270 nm. As this phenomena is blue shifted, as R diminishes, a second zero dispersion is attained at R=210 nm.

4.3. Silica Nanowire

The properties which have been observed for the nanowire composed of Silica core and air cladding are briefly described here

4.3.1. Effective index

For a Silica circular optical waveguide, the variation of effective indices is observed as the radius of the waveguide is reduced and enters the nanowire regime. For the fundamental mode, variation in effective index with respect to core radius is shown in Fig. 4.16. The effective index η_{eff} satisfies equation (3.3) .Since the quasi-TM and TE fundamental H_{01}^{x} and H_{01}^{y} of the waveguide are degenerate for the circular optical waveguide the effective indices of H_{01}^{y} have not been presented here. Fig.4.16 further shows the higher order modes H_{11}^{x} (HE_{01} or LP_{11}), H_{21}^{x} (EH_{11} or LP_{21}), and $H\,_{02}^{x}$(HE_{21} or LP_{02}).

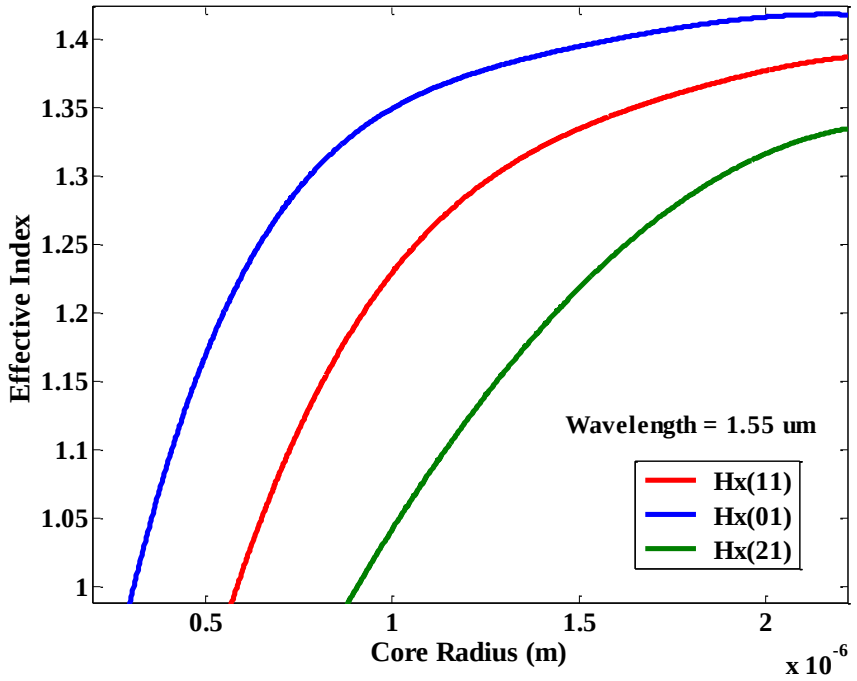

Fig. 4.16: Variation of the effective indices with the core radius.

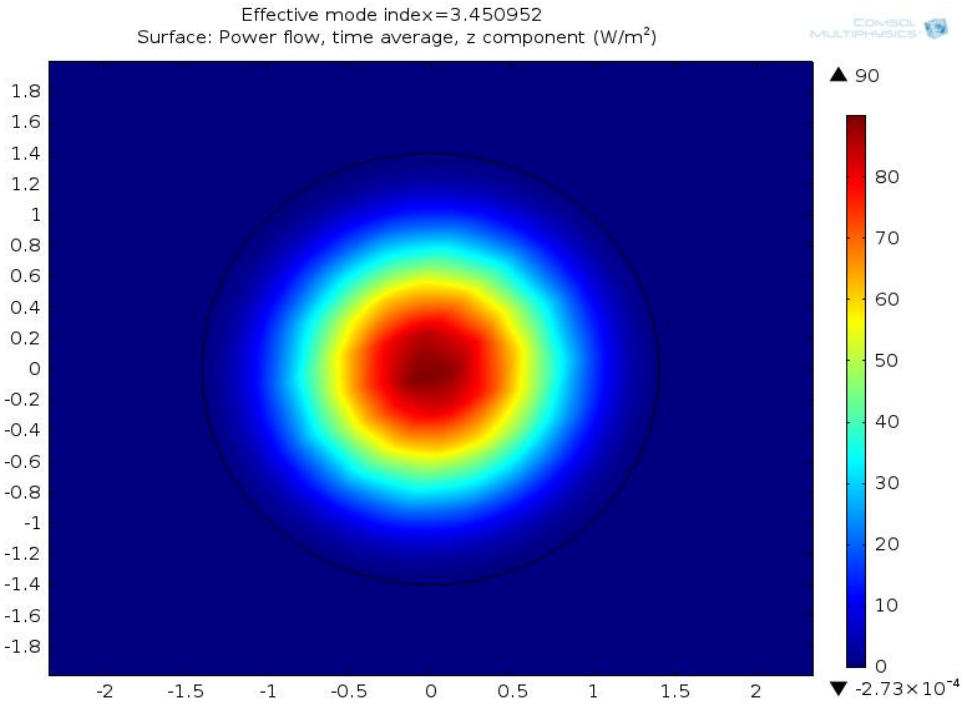

Fig. 4.17: Average power flow of H_{01}^{x} mode of z-component for Silica.

According to observation it is noted that initially as the core radius is decreased the effective indices of the modes decrease slowly but as the modes approach their cut-off conditions the indices decrease rapidly. With increasing radius the effective index asymptotically approaches that of the Silica while most of the optical power remain confined within the core. The effective index is simulated at a wavelength of 1.55 μm with core η_{core} =1.44 and η_{clad} =1 when core radius is 1.4 μm for Fig. 4.17.

4.3.2. Effective area

The variations of normalized effective area of both the fundamental mode and higher modes with respect to core radius is shown in Fig. 4.18. The effective area andnormalized effective area have been calculated from equations (3.9) and (3.10) respectively. From Fig.4.18 it can be noted that the fundamental mode being confined in the core has a lower normalized effective area than the higher modes. At first as the core radius is decreased the normalized effective areas of the modes increase to some extent but as the modes approach their cut-off conditions these increase rapidly. The normalized effective areas for the H_{11}^{x} and H_{21}^{x} modes increase as they approach their cutoff region. It is noted from Fig.4 that when the core radius is reduced, the H_{21}^{x} mode a pproaches the cutoff condition before H_{01}^{x} and H_{11}^{x} modes do.

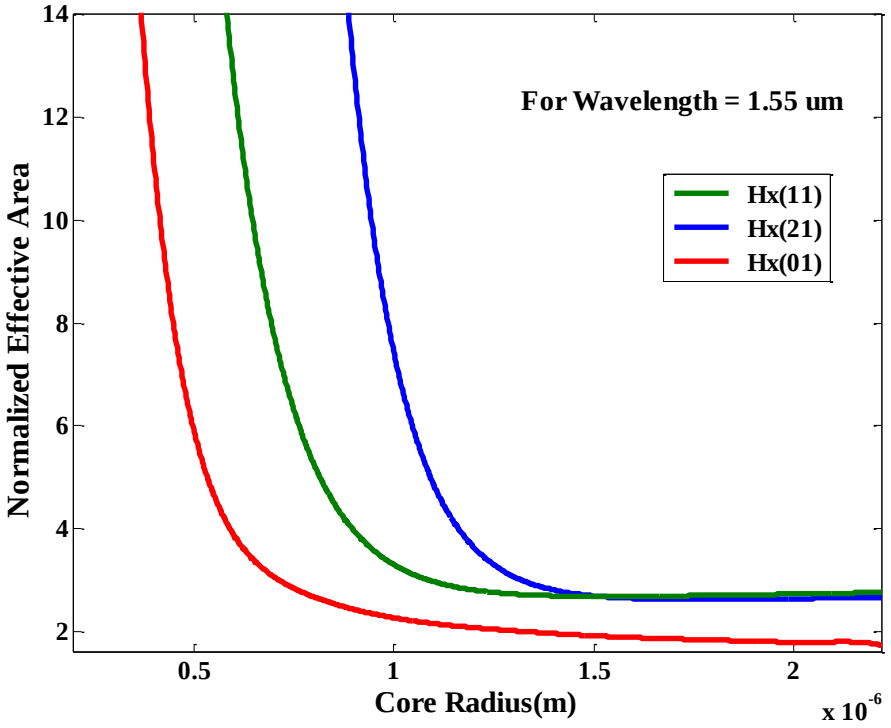

Fig. 4.18. Variation of the normalized Effective Area with the core radius.

4.3.3. Confinement factor

The comparison of the confinement factor with the core radius for fundamental mode and higher order modes is shown in Fig.4.19. Confinement Factor is calculated from the equation (3.9).

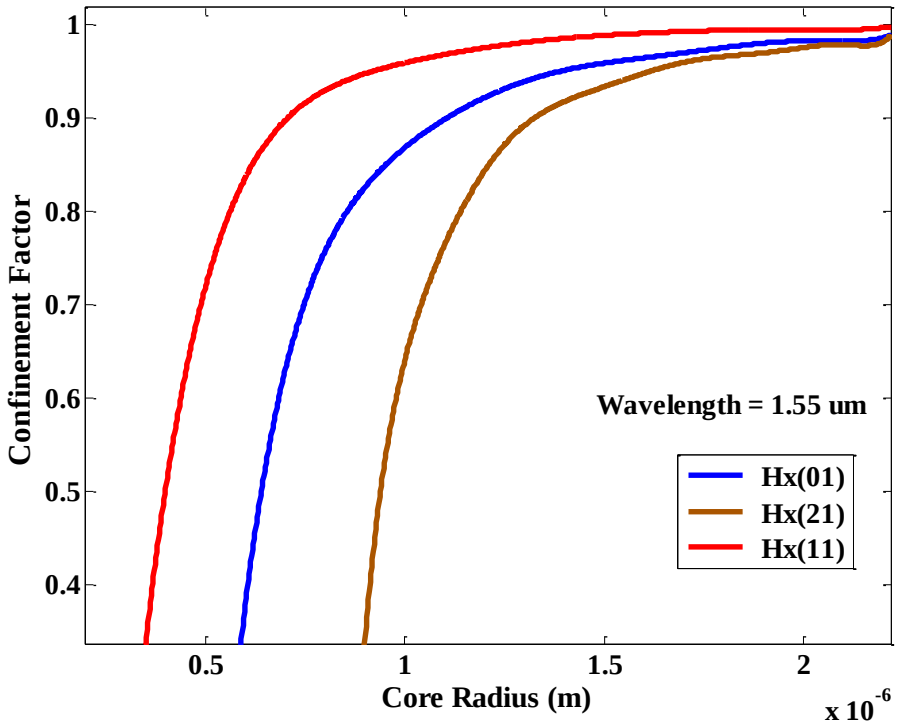

Fig. 4.19: Confinement factor for the fundamental and higher order modes.

It can be observed that the fundamental mode is near the cutoff region by the rapid increase in normalized effective area and also rapid decrease in the confinement factor beneath R=300 nm. It can also be noted from Fig. 4.19 that the cutoff radii for the H_{01}^{x}, H_{11}^{x} and H_{21}^{x} modes are approximately 300, 550, and 860 nm respectively.

4.4. Silica Nanowire for Optical Sensing

Based on wave guiding properties of optical nanowires discussed above, the nanowire waveguide is proposed to functionalize as sensing elements for detecting specimens in aqueous solutions. As shown in Fig. 4.20(a) a certain length of a silica nanowire is exposed to or immersed in the solution to be detected (highlighted in light green), and the wire guides light as a single-mode waveguide. When there is an index change (for example, caused by the addition of specimens, or just a temperature rise) around the wire, the guided light is changed in optical phase and intensity. To detect slight changes with high sensitivity, Mach-Zehnder interferometer based sensor system is used to coherently measuring the phase shift of the probing light [30]. As shown in Fig. 4.20(b), a Mach-Zehnder interferometer can be assembled with two uniform silica nanowires. One nanowire (nanowire 1 in the figure) is used as sensing arm with a certain length of sensitive area exposed to the measurand, and the other (nanowire 2) is used as reference arm that is kept in constant condition and is isolated from the measurand and both arms are immersed in aqueous solution. A probe light that is launched through the nanowire propagates through the first 3 dB coupler, operating as an optical splitter, which divides it between the sensing and the reference arms. It finally recombines via the second 3 dB coupler, working as an optical combiner, as shown in Fig. 4.21.

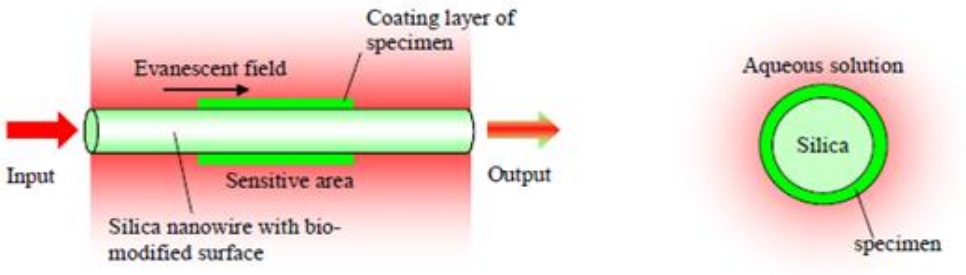

(a) **(b)**

Fig. 4.20: Schematic diagram of (a) a silica nanowire for selective sensing and (b) a cross section view of the composite waveguide [29].

The phase shift caused by the index change due to the specimen placed in the sensing arm is measured by the interferometer and the information of the specimens can thus be retrieved.

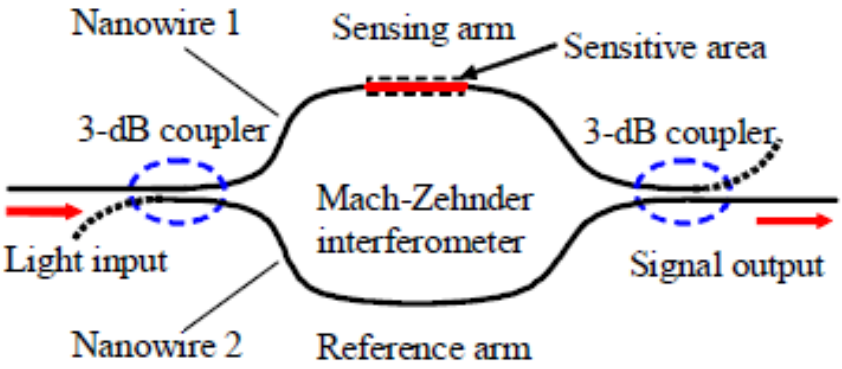

Fig. 4.21: A sensor with a Mach-Zehnder interferometer [29].

The refractive index of the single-mode silica nanowire and the aqueous solution (water) were considered to be 1.482 and 1.355, respectively, at an operating wavelength of 325 nm [59], [60]. The specimen was assumed to be nanoparticles of 12 nm thickness with a refractive index value of 1.4 (Polystreptavidin) [16].

4.4.1. PML thickness

The perfectly matched layer (PML) introduced by Berenger [61] is widely accepted as an efficient numerical absorber used in time-domain electromagnetic (EM) solvers. PML is widely used and has become the absorbing boundary technique of choice in much of computational electromagnetism. PML is used for reflectionless absorption of electromagnetic waves irrespective of their frequency and angle of incidence [62], which can be employed as an alternative to the transparent boundary condition (TBC). To provide reflectionless absorption of the incident fields for the finite-difference time-domain (FDTD) method, in recent years, the PML is popularly employed as the boundary condition for the Eigen mode analysis of the leaky waveguide modes. For the analysis of nanowire structure PML is used. It does not have a practical existence. It is used only for analysis purpose to enhance the accuracy of the analysis. It is of the same refractive index of cladding which is in this structure aqueous solution. The thickness of PML is main concern in this design. The thickness of PML is determined from the curve of Fig. 4.22, for core radius of 500nm using wavelength = 325 nm. From this curve, from when thickness of PML is 25 nm, effective index become stable.

Throughout this design thickness of PML is used = 25 nm for both reference arm and sensing arm.

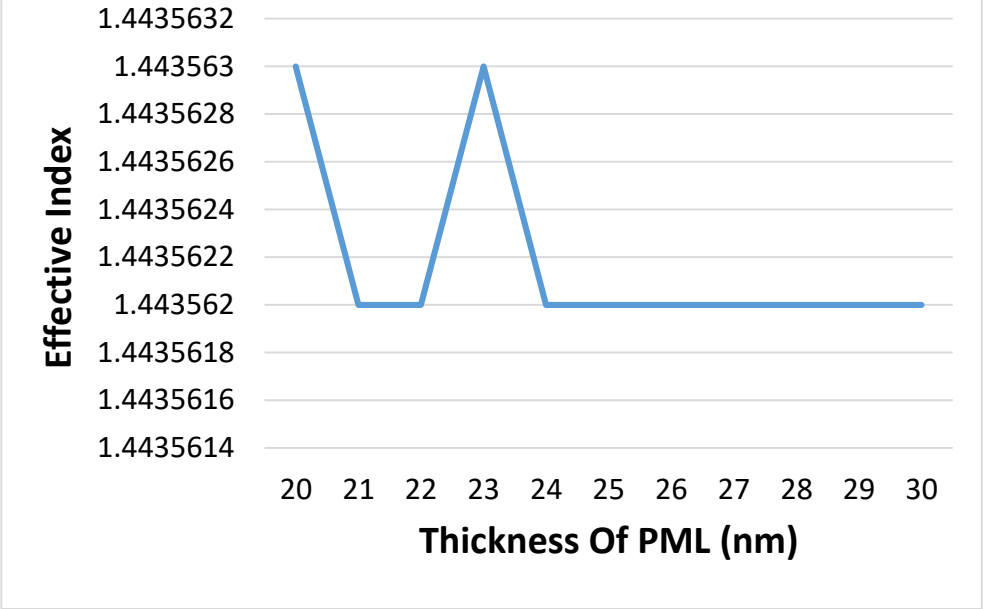

Fig. 4.22: Change in effective index with respect to thickness of PML

4.4.2. Propagation constant

The variation of the propagation constant β (μm^{-1}) in the reference arm and the propagation constant difference Δβ (μm^{-1}) between the two arms with respect to the silica nanowire radius has been examined. The results are presented in Fig. 4.23(a) and Fig 4.23(b) respectively where β satisfies equation (3.2).

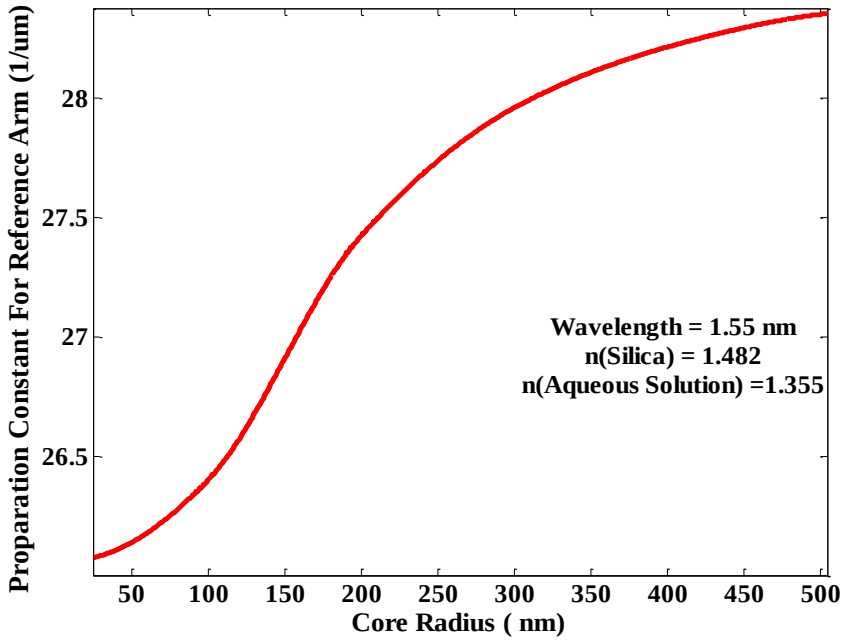

(a)

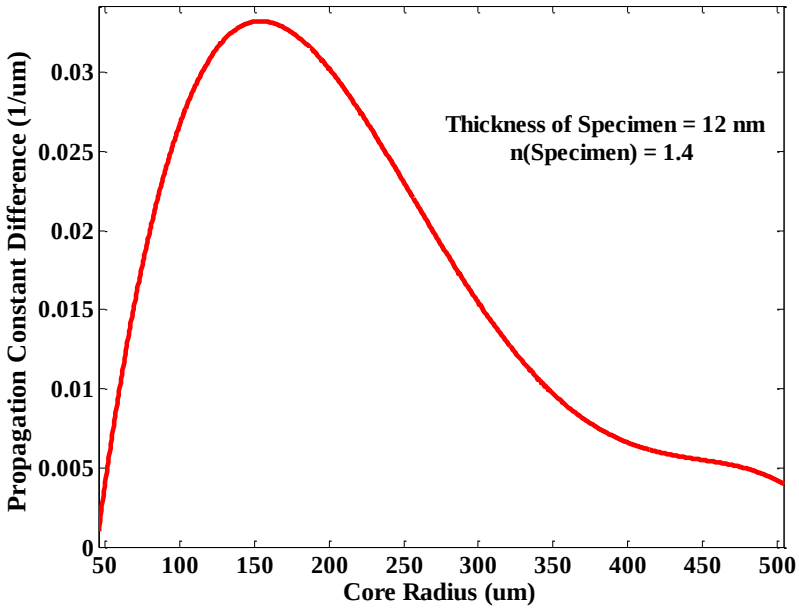

(b)

Fig. 4.23: (a) Propagation constant of the reference arm and (b) propagation constant difference Δβ (between the reference and sensing arms) as a function of the fiber radius.

Both the curve is plotted against core radius, over the range from 50 nm to 500 nm. For Fig. 4.23(a) as radius of the core decreases, β also reduces, and the rate of reduction slowly increases. However, when close to cut of the propagation constant reduces at a lower rate for a core radius below 125 nm. From Fig. 4.23(b), Δβ initially increases with the increase of the core diameter. However, for a core radius about 150 nm, it exhibits a peak value, and as the core diameter increases further, Δβ reduces.

4.4.3. Comparison in power fracion in reference arm and sensing arm

Further, the power fraction in the aqueous solution (water) for the reference and the sensing arm has also been studied with the variation of the nanowire core radius and the result is presented in Fig.4.24.The power fraction in the aqueous solution decreases in the both arms with the increase of the core diameter since the field is more confined in the core region, with the power fraction in the sensing arm being slightly lower. For a core radius of about 125 nm, near the cutoff value of the optical mode, the field extends mostly in the cladding (aqueous) region. Around the core radius of about 150 nm, nearly 50% of the power lies in the aqueous solution for both the reference and the sensing arms.

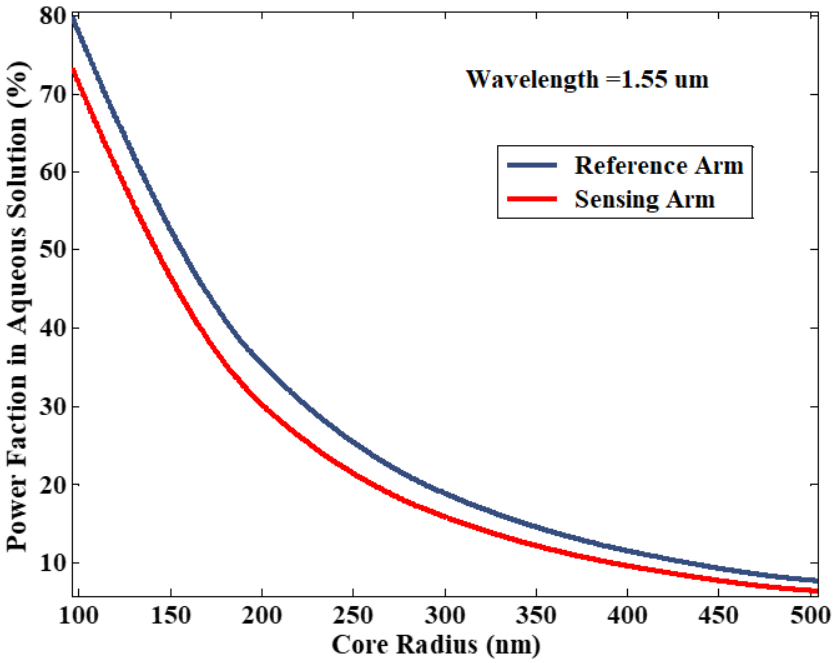

Fig. 4.24: Power fraction for aqueous solution for the sensing and the reference arms as a function of the fiber radius (um).

4.4.4. Power Fraction in Sensing Arm

The power fraction in the different optical media of the sensing arm with the variation of the nanowire core radius has also been analyzed and results are presented in Fig. 4.25.

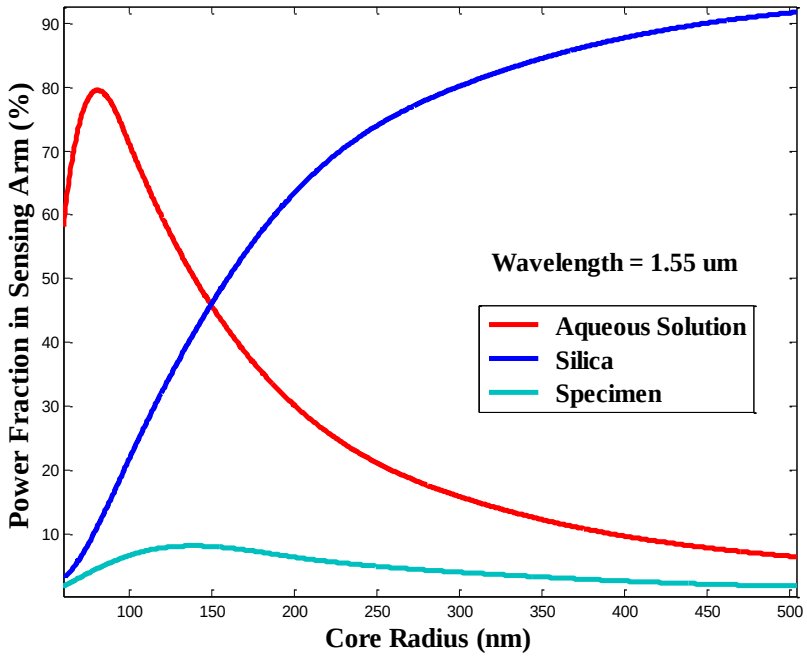

Fig.4.25: Power fraction of the sensing arm as a function of the fiber radius for a specimen index.

For a small core diameter, the power fraction is minimum in the core and maximum in the specimen and aqueous solution regions. As the core diameter increases, the power fraction in the core and aqueous solution regions of the sensing arm cross over when core radius about 150 nm, and the power fraction in the core and the aqueous solution become maximum and minimum respectively with the increase of core radius. The power in the specimen exhibits a peak near a core radius of around 150 nm and above that decreases to zero.

4.4.5. Propagation constant difference for different specimen indices

The propagation constant difference $\Delta\beta$ (μm^{-1}) between the reference and the sensing arm with the nanowire fiber radius have been examined for different refractive index values in Fig. 4.26.

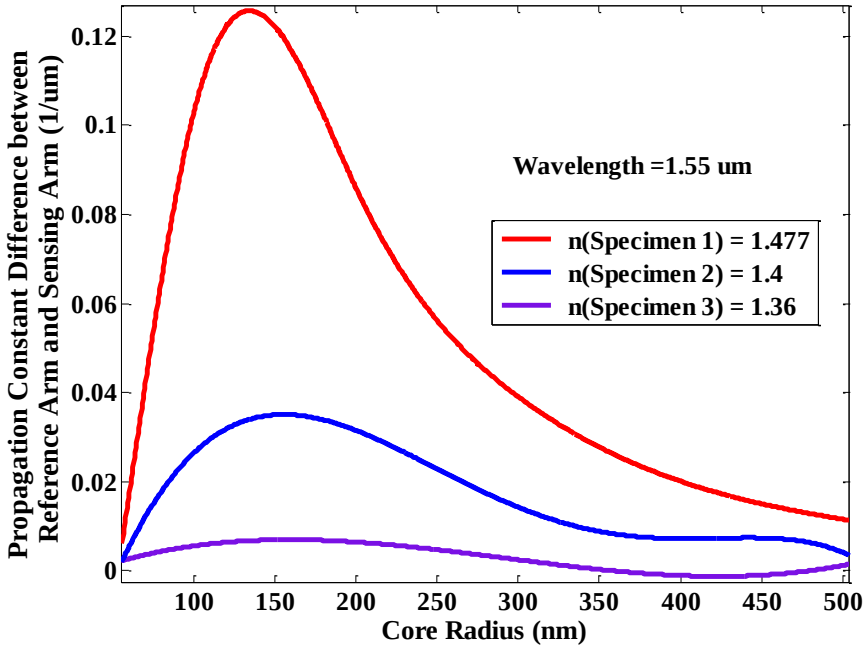

Fig.4.26: Change in propagation constant as a function of the fiber radius for different specimen indexes.

For all the specimen refractive index values, the change in the propagation constant initially increases, reaching a peak value at a fiber radius of about 150 nm and finally decreases. For a specimen refractive index n_s=1.477 near the core refractive index (= 1.482), $\Delta\beta$ is higher compared to $\Delta\beta$ for a specimen with a refractive n_s=1.36 index near to that of the aqueous solution (=1.355).

4.4.6. Propagation constant and power fraction in the specimen

The change in the propagation constant difference $\Delta\beta$ (μm^{-1}) between the reference and

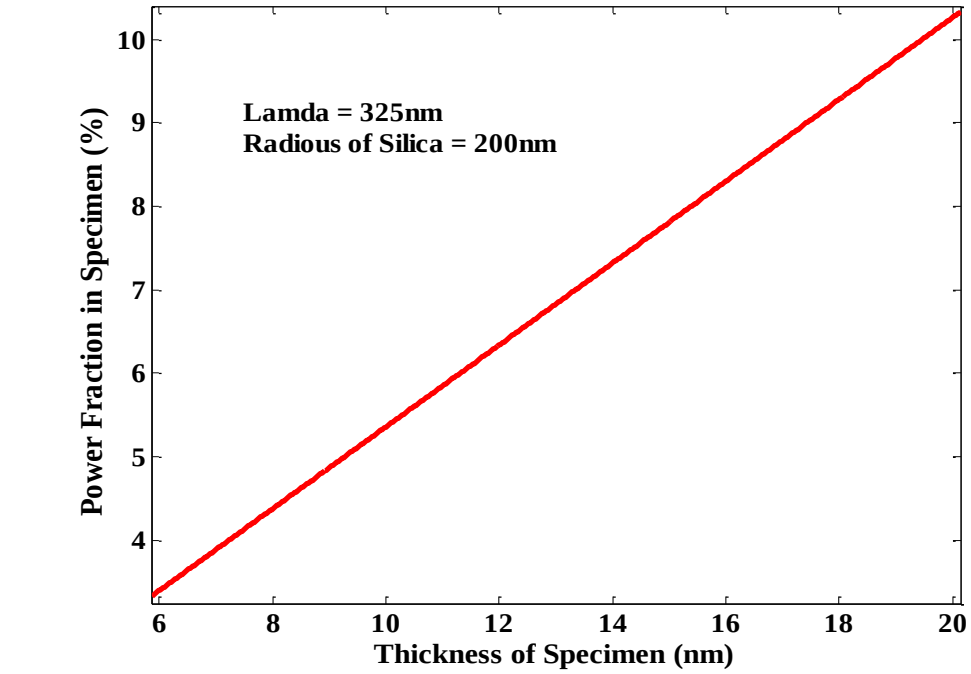

(a)

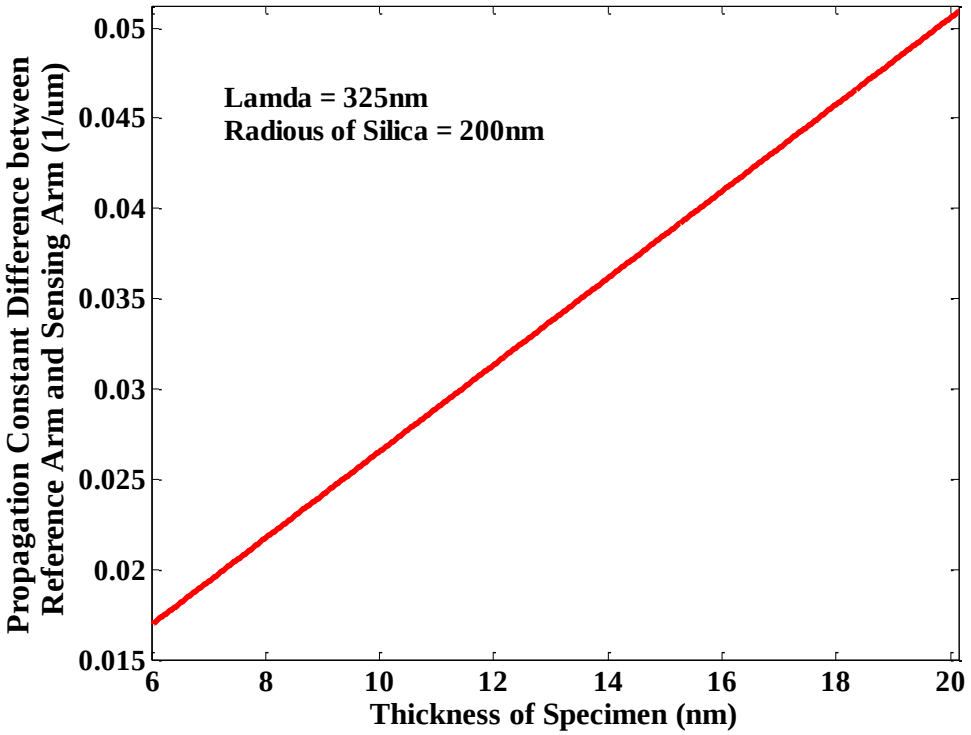

(b)

Fig.4.27: (a) Change in propagation constant and (b) power fraction in the specimen with the variation of the specimen thickness.

sensing arms and the power fraction in the specimen as a function of the specimen thickness, for a core radius of 200 nm, have been investigated in Fig. 4.27. The propagation constant of a mode in a waveguide, determines how the amplitude and phase of that light with a given frequency varies along the propagation direction.

4.5. Sensitivity

The phase shift (ΔΦ) of the sensing arm can be obtained as,

$$\Delta\Phi = (\beta - \beta_0) \cdot L = \Delta\beta \cdot L \tag{4.1}$$

Where L is the effective length of the sensitive area, β_0 and β are the initial and instant propagation constants of the light in the sensitive area, respectively**.** At a given temperature and pressure, when a certain amount of the specimen with initial refractive index $n_{s0} = 1.4$ is added into a solution (water) with an refractive index of $n_c = 1.355$ the overall index n_s as can be approximately obtained as,

$$n_s = n_c \,.(1-C) + n_{s0} \,.C \tag{4.2}$$

C the molar concentration of the specimen in the solution.

The sensitivity of sensors can be normalized [29],

$$S_N = \frac{1}{L} \,. \frac{d\,(\Delta\Phi)}{dn_s} \tag{4.3}$$

which can be written as,

$$S_N = \frac{d\Delta\beta / dC}{dn_s / dC} \tag{4.4}$$

4.5.1. Change in propagation constant with molar fraction

From the equation (2) for different molar concentration (C) ranging from 10^{-4} M to 10^{-1} M overall refractive index n_s of the specimen to be dictated has been determined. For this n_s propagation constant has been analyzed and C-dependent Δβ (μm^{-1}) has been obtained in Fig. 4.28 in which two curve corresponding to core radius 100 nm and 200 nm respectively. It shows that Δβ increases linearly with molar concentration (C) we concerned.

For, R = 100 nm, Slope of the curve = $^{d\Delta\beta}/_{dC}$ = 0.042 μm^{-1} (approximately)

For R = 200 nm, Slope of the curve = $^{d\Delta\beta}/_{dC}$ = 0.032 μm^{-1} (approximately)

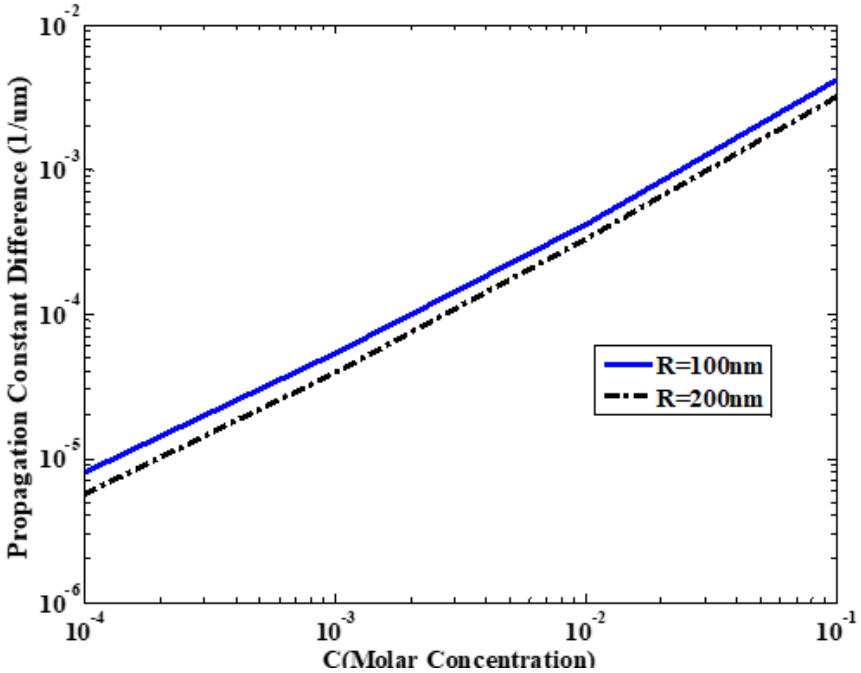

Fig.4.28: Changes in propagation constant (Δβ) as a function of molar concentration (*C*) of the specimen.

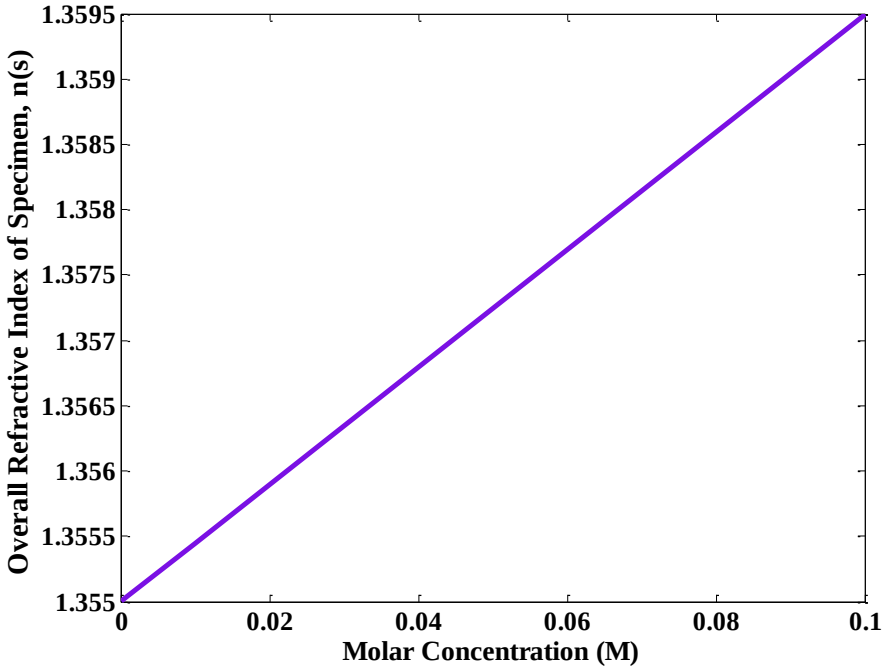

Fig.4.29: Change of specimen index with respect to molar concentration (M)

From Fig.4.29, Slope = $^{dn_s}/_{dC}$ = .045

From equation (4.4),

For R = 100 nm

$S_N = \frac{0.042\ \mu m^{-1}}{.045} = .933\ \mu m^{-1}$

For phase shift $\Delta\varphi = 2\times 10^{-3}\pi$

Length of Sensitive area = $\frac{\Delta\varphi}{\Delta\beta} = \frac{2\times 10^{-3}\pi}{0.042\ \mu m-1} = 150$ nm.

For R = 200 nm

$S_N = \frac{0.032\ \mu m^{-1}}{.045} = .711\ \mu m^{-1}$

For phase shift $\Delta\varphi = 2\times 10^{-3}\pi$

Length of Sensitive area = $\frac{\Delta\varphi}{\Delta\beta} = \frac{2\times 10^{-3}\pi}{0.042\ \mu m-1} = 197$ nm.

From this calculation, it can be said that S_N increases with the decreasing of the wire radius, indicating that thinner wires provide higher sensitivity which reduces the length of the sensitive area.

CHAPTER 5

CONCLUSION

5.1. Conclusion of the Work

In this work, properties of silicon nanowire and silica nanowire have been presented using software based on finite element method. Due to presence of all six components, the nanowires having small radii are fully vectorial. Hence, the modal solutions of the optical waveguides were approached with fully vectorial formulation. Study of characteristics of both silicon nanowire and silica nanowire are presented in the work. These characteristics include variations of effective indices, effective area, dispersion, power confinement etc. for the fundamental mode H_{01}^{x} and higher order modes H_{01}^{x}, H_{11}^{x} and H_{02}^{x} of silicon nanowire and silica nanowire. The modal asymmetry of the higher order can have an impression on the coupling between two nanowires and on sensor-based devices.

The study shows while all three components of H-field are continuous across the dielectric interfaces, the electric field components are not. It has further been shown in this work that the modes in such nanowires with strong index contrast have hybridness or show the presence of the non-dominant orthogonal polarization. It has been noted in case of waveguides with small dimensions that the dispersion properties can be greatly controlled for various linear and non-linear application. The non-linear properties of silicon nanowire have also been studied in this work.

Afterwards a detailed study of optical sensing of the nanowires have been presented. A Mach-zender based optical sensor have been studied for this part. A phase shift has been noted due to the presence of a sensing arm and a reference arm in the sensor. Assuming the specimen to be polystreptavidin, characteristics like propagation constant, propagation constant difference and power fraction have been studied and plotted against variations of core diameters. The sensitivity of the optical sensor have been studied against variations of the molar concentration for two different radii of

nanowire range. The concept of ‘the thinner the wire, the higher the sensitivity’ have been presented in this work. Finally, the study has suggested that optical sensing with nanowires may set forth a new approach to miniaturized optical sensors with high sensitivity.

5.2. Future Scope of Work

Nanotechnology has a huge scope in the coming generations, and there is always room for improvement in every nanowire related work. Many new discoveries are expected in the short run basing on the uniqueness of nanowire building blocks. The nanowire technology can be used for applications in the three different effects such as Self-Phase Modulation (SPM), Cross-Phase Modulation (CPM) and Four-Wave Mixing (FWM). At high power level, nanowire technology can be further developed for stimulated effects such as Stimulated Brillouin-Scattering (SBS) and Stimulated Raman-Scattering (SRS). The sensitivity parameter of nanowires desire much opportunities to be enhanced. The reduced footprint of the nanowire sensor may allow sensing in environment of smaller scale, support integration of sensor array with higher density, and require fewer samples. But in practice, to realize a nanowire sensor modeled in this work, some challenges such as instability of the nanowire-assembled couplers and oversensitivity of the whole system has to be overcome, which require further experimental investigation in the future. The optical sensing part of the work can be made further refined in future by studying with sensors made up of different specimens to designate the best among them. Other properties of nanowire as biosensors can also be explored in future works. Studies relating to improvement of performance and stability of nanowires while making them more cost-effective will go a long way in the growth of nanowire technology.

References

[1] [Online]. Available: http://whatis.techtarget.com/definition/nanowire.

[2] [Online]. Available: https://en.wikipedia.org/wiki/Nanowire.

[3] E. Meng, W. Li, K. Nakane, Y. Shirahashi, Y. Hayakawa, and H. Tatsuoka., "Shape modification of Si nanowires by using faceted silicide catalysts nucleated in Au-Si catalyst solution during the growth." [Online]. Available: http://aip.scitation. org/doi/full/10.10.63/1.4821119.

[4][Online].Available:https://www.coursera.org/learn/nanotechnology2/lecture/pwvla/ definition-and-properties-of-nanowires.

[5] Jahwarhar Izuan Abdul Rashid, Jaafar Abdullah, Nor Azah Yusof, and Reza Hajian, "The Development of Silicon Nanowire as Sensing Material and Its Applications," *Journal of Nanomaterials,* vol. 2013 (2013), Article ID 328093, pp. 16, 2003.

[6] G. Tian, K. Pan, Y. Chen et al., "Vertically aligned anatase TIO_2 nanowire bundle arrays: use as Pt support for counter electrodes in dye-sensitized solar cells," *Journal of Power Sources*, vol. 238, pp. 350–355, 2013.

[7] F. Shahdost-fard, A. Salimi, E. Sharifi, and A. Korani, "Fabrication of a highly sensitive adenosine aptasensor based on covalent attachment of aptamer onto chitosan-carbon nanotubes-ionic liquid nanocomposite," *Biosensors and Bioelectronics*, vol. 48, pp. 100–107, 2013.

[8] L. Qian, J. Mao, X. Tian, H. Yuan, and D. Xiao, "In situ synthesis of CuS nanotubes on Cu electrode for sensitive nonenzymatic glucose sensor," *Sensors and Actuators B*, vol. 176, pp. 952–959, 2013.

[9] Y. Ding, Y. Liu, J. Parisi, L. Zhang, and Y. Lei, "A novel NiO-Au hybrid nanobelts based sensor for sensitive and selective glucose detection," *Biosensors and Bioelectronics*, vol. 28, no. 1, pp. 393–398, 2011.

[10] Y. Sun, S. H. Yang, L. P. Lv et al., "A composite film of reduced graphene oxide modified vanadium oxide nanoribbons as a free standing cathode material for rechargeable lithium batteries," *Journal of Power Sources*, vol. 241, pp. 168–172, 2013.

[11]H. Lee, J. Hong, S. Lee, S. D. Kim, Y. W. Kim, and T. Lee, "Selectively grown vertical silicon nanowire p−n+ photodiodes via aqueous electroless etching," *Applied Surface Science*, vol. 274, pp. 79–84, 2013.

[12] A. Gao, N. Lu, P. Dai et al., "Silicon-nanowire-based CMOS-compatible field-effect transistor nanosensors for ultrasensitive electrical detection of nucleic acids," *Nano Letters*, vol. 11, no. 9, pp. 3974–3978, 2011

[13] J. Y. Oh, H. Y. Jang, W. J. Cho, and M. S. Islam, "Highly sensitive electrolyte-insulator semiconductor pH sensors enabled by silicon nanowires with Al_2O_3/SiO_2 sensing membrane," *Sensors and Actuators B*, vol. 171, pp. 238–243, 2012.

[14] J. Bae, H. Kim, and X. M. Zhang, "Si nanowire metal-insulator-semiconductor photodetectors as efficient light harvesters," Nanotechnology, Article ID 095502, p. 21, 2010.

[15] P. K. Kim, S. J. Cho, J. Sung, H. S. Oh, and G. Lim, "Bio-molecules detection sensor using silicon nanowire," in The 2nd International Conference on Smart Materials and Nanotechnology in Engineering, vol. 7493 of Proceedings of SPIE, SPIE, Weihai, China, 2009.

[16] J. H. Choi, H. Kim, H. S. Kim et al., "MMP-2 detective silicon nanowire biosensor using enzymatic cleavage reaction," *Journal of Biomedical Nanotechnology*, vol. 9, pp. 732–745, 2013.

[17] A. A. Talin, L. L. Hunter, F. Ĺonard, and B. Rokad, "Large area, dense silicon nanowire array chemical sensors," *Applied Physics Letters*, vol. 89, no. 15, Article ID 153102, 2006.

[18] K.-I. Chen, B.-R. Li, and Y.-T. Chen, "Silicon nanowire field-effect transistor-based biosensors for biomedical diagnosis and cellular recording investigation," *Nano Today*, vol. 6, no. 2, pp. 131–154, 2011.

[19] O. A. Sadik, S. K. Mwilu, and A. Aluoch, "Smart electrochemical biosensors: from advanced materials to ultrasensitive devices," *Electrochimica Acta*, vol. 55, no. 14, pp. 4287–4295, 2010.

[20] [Online]. Available: http://www.understandingnano.com.

[21] [Online]. Available: https://en.wikipedia.org/wiki/Waveguide_(optics).

[22] M. H. weik, *Fiber Optics standard dictionary*, Springer-science+business media, B. V, 3rd edition.

[23] John M. Senior, Optical Fiber Communications Principles and Practice, 3rd edition.

[24] L. M. Tong, J. Y. Lou, and E. Mazur, "Single-mode guiding properties of subwavelength diameter silica and silicon wire waveguides," *Opt. Express*, vol. 12, pp.

1025–1035,2004. [Online]. Available: http://www.opticsexpress.org/abstract.cfm?URI =OPEX-12-6-1025.

[25] L. M. Tong, R. R. Gattass, J. B. Ashcom, S. L. He, J. Y. Lou, M. Y. Shen, I. Maxwell, and E. Mazur, "Subwavelength-diameter silica wires for low-loss optical wave guiding," *Nature*, vol. 426, pp. 816–819, 2003.

[26] [Online]. Available: https://www.intechopen.com/books/nanowires-fundamental-research/four-wave-mixing-in-silicon-nanowire-waveguides-and-its-applications-in-wavelength-conversion

[27] J. B. Driscoll, X. Liu, S. Yasseri, I. Hsieh, J. I. Dadap, and Richard M. Osgood, Jr., "Large longitudinal electric fields (Ez) in silicon nanowire waveguides," *Opt. Express*, vol. 17, no. 4, pp. 2797-2804, 2009.

[28] N. Kejalakshmy, A. Agrawal, Y. Aden, D. M. H. Leung, B.M.A. Rahman, K.T.V. Grattan, "Characterization of silicon nanowire by use of full-vectorial finite element method," *Applied Optics*, vol. 49, no. 16, pp. 3173-3181, 2010.

[29] J. Y. Lou, L. M. Tong, and Z. Z. Ye, "Modeling of silica nanowires for optical sensing," *Opt. Express*, vol. 13, pp. 2135-2140, 2005.

[30] C. Themistos, M. Rajarajan, B. M. Azizur Rahman, and K. T. V. Grattan, "Characterization of silica nanowires for optical sensing," *J. Lightwave Technol.*, vol. 27, no. 24, pp. 5537- 5542, 2009.

[31] J. Wang and D. Dai, "Highly sensitive Si nanowire-based optical sensor using a Mach– Zehnder interferometer coupled microring," *Opt. Lett.*, vol. 35, no. 24, pp. 4229-4231, 2010.

[32] Mohammad Mohebbi, Hadi Khormaei, and Rasul Rezaei, "Modeling of an optical Sensor for Detection of Nanoparticles at 1550nm," 2012.

[33] [Online].Available:https://www.engr.uvic.ca/mech410/lectures/FEA_Theory.pdf.

[34] G. P. Nikishkov, *Introduction to the Finite Element Method* [Online]. Available: http://citeseerx.ist.psu.edu/viewdoc/download?doi=10.1.1.521.9293&rep=rep1&type=pdf

[35] [Online]. Available: http://web.mit.edu/16.810/www/16.810_L4_CAE.pdf.

[36] [Online]. Available: http://www.open.edu/openlearn/science-maths-technolgy/int--roduction-finite-element-analysis/content-section-1.7.

[37] [Online]. Available: https://en.wikipedia.org/wiki/COMSOL_Multiphysics.

[38] [Online]. Available: http://faculty.washington.edu/finlayso/Finlayson_ paper_61 1d.pdf.

[39] [Online]. Available: https://www.sp.se/en/index/services/calculations/comsolmul--tiphysics/Sidor/default.aspx.
[40] [Online]. Available: https://www.materialstoday.com/computation-theory/produ--cts/comsol-multiphysics-44.
[41] [Online]. Available: https://people.rit.edu/pnveme/personal/VenkatCOMSOL42/IntroductionCOMSOL/index.html.
[42] [Online]. Available: http://www.worldscientific.com/worldscibooks /10.1142 /6141.
[43] [Online]. Available: http://www.comsol.com/blogs/what-is-comsol-multiphysics.
[44] [Online]. Available: https://www.comsol.com/forum/thread/25969/advantages-of-comsol?last=2012-02-08T18:20:22Z
[45] [Online].Available: https://www.comsol.com/blogs/how-to-implement-meshrefinement-study.
[46] [Online]. Available: http://www.fiber-optics.info/articles/types_of_optical_fiber.
[47] [Online]. Available: https://www.multicominc.com/training/technical-resources/single-mode -vs-multi-mode-fiber-optic-cable.
[48] [Online]. Available: http://www.infocellar.com/networks/fiber-optics/fiber.html.
[49] [Online]. Available: https://www.rp-photonics.com/ effectiverefractiveindex.html.
[50] [Online]. Available: https://www.rp-photonics.com/spotlight_2007_10_07.html.
[51] [Online]. Available: http://www.npl.co.uk/upload/pdf/aeff_ver3.pdf.
[52] [Online]. Available: https://www.fibercore.com/fiberpaedia/confinement-factor.
[53] Volkmar Brückner, Senior Experten Service Bonn and HfT Leipzig, *To the use of Sellmeier Formula*, Germany. [Online]. Available: http://www.springer.com/cda/content/document/cda_downloaddocument/v_37_6493.pdf?SGWID=0-0-45-1364639-p174303219.
[54] P. Klocek, *Handbook of infrared optical materials* (Marcel Dekker, New York, NY 1991).
[55] E. D. Palik, Handbook of optical constants of solids (Academic Press, New York, NY 1998).
[56] [Online]. Available: http://jpier.org/PIER/pier73/13.07040201.Singh.S.pdf.
[57] [Online]. Available: https://www.rp-photonics.com/passive_fiber_optics11.html.
[58] [Online]. Available: https://www.fiberoptics4sale.com/blogs/archive-post/95052678-what-is-optical-fiber-dispersion.
[59] [Online]. Available: http://www.mtel.cz/eng/analysis.php.

[60] E. Udd, *Fiber Optic Sensors: An Introduction for Engineers and Scientists* John Wiley & Sons, New York, 1991.
[61] J. P. Berenger, “A perfectly matched layer for the absorption of electromagnetic waves,” *J. Comput. Phys.*, vol. 114, pp. 185–200, 1994.
[62] [Online]. Available:https://optiwave.com/optibpm-manuals/bpm-perfectly-matched-layer-pml.